Electronic Supplementary Information for

Structure Property Relationship in Multi-Stimuli Responsive BODIPY-biphenyl-Benzodithiophene TICT Rigidochromic Rotors Exhibiting (pseudo) Stokes Shift up to 221 nm

Sushil Sharma[a], Zimu Wei[b], Ferdinand C. Grozema[b] and Sanchita Sengupta[a]*

[a]Department of Chemical Sciences, Indian Institute of Science Education and Research (IISER) Mohali, Punjab-140306, India.

[b]Department of Chemical Engineering, Delft University of Technology, Van der Maasweg 9, 2629, HZ Delft, The Netherlands

*Email: sanchita@iisermohali.ac.in

Table of contents

1. Synthesis

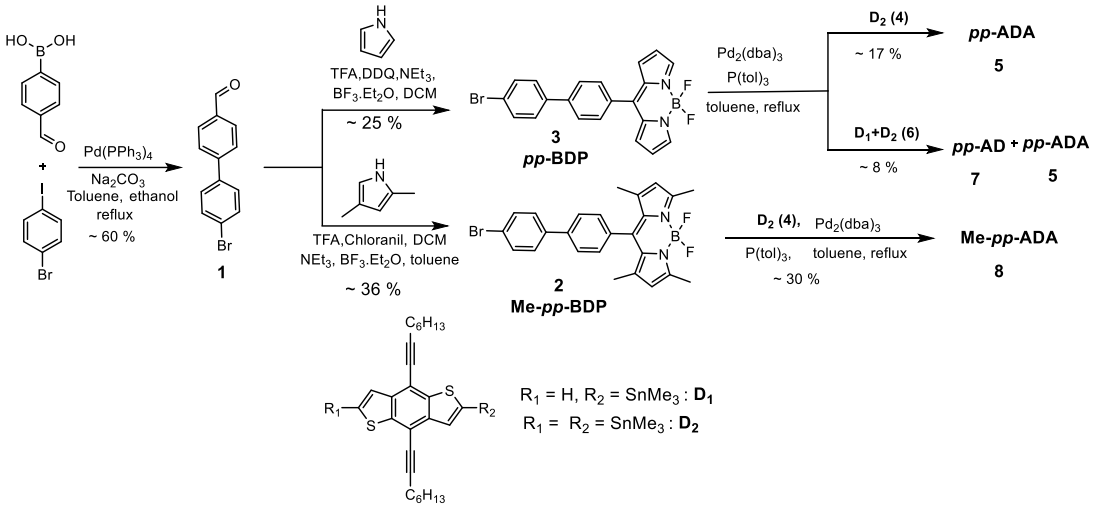

Scheme S1. Synthesis of ***pp*-AD**, ***pp*-ADA** and **Me-*pp*-ADA**.

D₁ and **D₂** were synthesized according to previously reported procedure starting from thiophene-3-carboxylic acid.[S1]

Synthesis of 4'-bromo-[1,1'-biphenyl]-4-carbaldehyde (1):

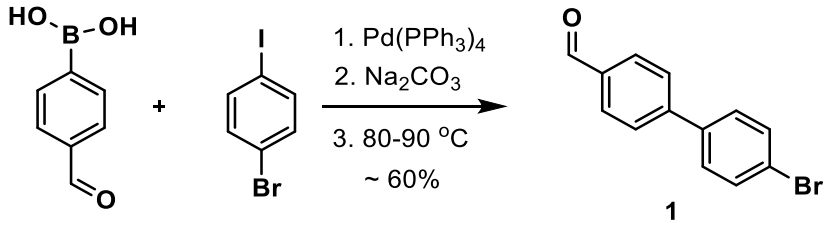

Scheme S2. Synthesis of 4'-bromo-[1,1'-biphenyl]-4-carbaldehyde.[S2]

To a solution of 1-bromo-4-iodobenzene (2 g, 7.06 mmol) in toluene, catalytic amount of tetrakis-triphenylphosphinepalladium $Pd(PPh_3)_4$ (3-5 mol%) was added followed by addition of 5 mL aqueous solution of K_2CO_3 (2M). A solution of 4-formyl phenyl boronic acid (1 g, 6.66 mmol) in 15 mL ethanol was added to reaction mixture and the mixture was heated to reflux for 5 hours (h). After cooling to room temperature, the reaction mixture was extracted with $CHCl_3$ and washed with brine solution. Subsequently, the organic layers were passed through sodium sulphate and solvent was evaporated on rotary evaporator. The crude product

was purified by column chromatography using 90:10 hexane:ethylacetate to obtain white solid with 60% yield.

^{1}H NMR (400MHz, $CDCl_3$) δ (ppm): 10.06 (s, 1 H), 7.95 (d, *J* = 8 Hz, 2 H), 7.72 (d, *J* = 8 Hz, 2 H), 7.61 (d, *J* = 8 Hz, 2 H), 7.50 (d, *J* = 8 Hz, 2 H).

Synthesis of Me-*pp*-BODIPY (2):

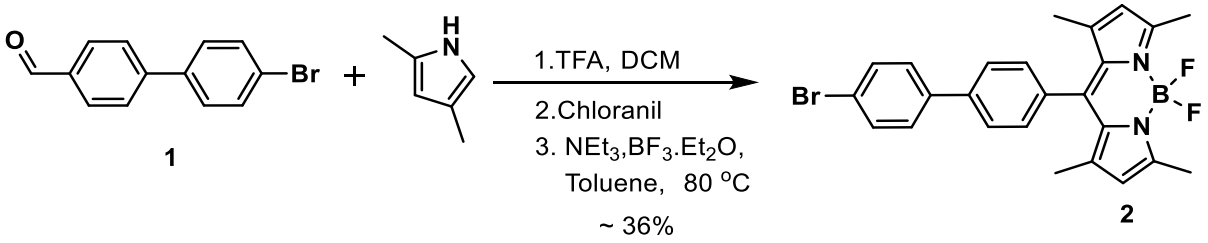

Scheme S3. Synthesis of **Me-*pp*-BODIPY** compound **2**.[S3]

Compound **1** (100 mg, 0.38 mmol) was dissolved in dry dichloromethane (DCM) and purged. Pyrrole (127 mg, 1.34 mmol) and 3-4 drops of trifluoroacetic acid was added and the reaction mixture was stirred for 5 h at room temperature. Subsequently, chloranil (102 mg, 0.41 mmol) was added and stirred for 40 minutes. The reaction intermediate was passed through silica column using DCM and solvent was evaporated to collect the crude intermediate. Toluene was added followed by addition of triethylamine (776 mg, 7.67 mmol) and reaction mixture was stirred. After 15 minutes, boron trifluoride diethyl etherate ($BF_3.Et_2O$) (1.3 g, 9.1 mmol) was added and stirred at 80 °C for 40 minutes and reaction was monitored by TLC. The extraction was done by ethyl acetate and the product was purified by column chromatography using DCM and hexane as eluent to obtain orange solid in 36% yield.

^{1}H NMR (400MHz, $CDCl_3$) δ (ppm): 7.71 (d, *J* = 8 Hz, 2 H), 7.61 (d, *J* = 8 Hz, 2 H), 7.54 (d, *J* = 8 Hz, 2 H), 7.36 (d, *J* = 8 Hz, 2 H), 5.99 (s, 2 H), 2.56 (s, 6 H), 1.43 (s, 6 H).

Synthesis of *pp*-BODIPY (3):

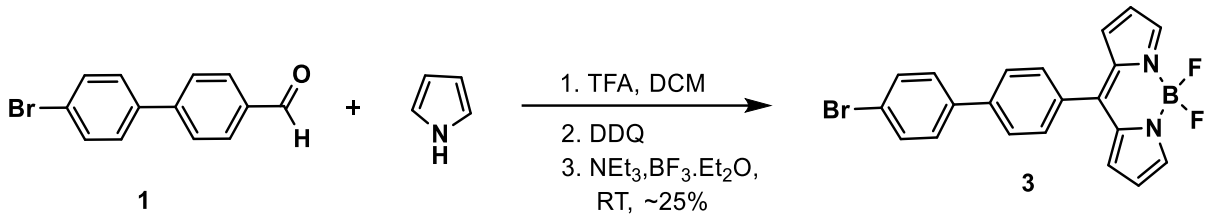

Scheme S4. Synthesis of ***pp*-BODIPY**.[S4]

Compound **1** (200 mg, 0.77 mmol) was dissolved in dry DCM and purged nitrogen. Then pyrrole (0.16 mL, 2.31 mmol) and catalytic amount of trifluoroacetic acid and stirred for 1 h at room temperature under nitrogen atmosphere. 2,3-Dichloro-5,6-dicyano-1,4-benzoquinone (DDQ) (174.8 mg, 0.77 mmol) was added to the reaction mixture and stirred for 0.5 h and further 6 mL of triethylamine was added followed by addition of $BF_3.Et_2O$ (6 mL) and stirred for 3 h at room temperature. The organic phase was washed by saturated solution of Na_2CO_3, dried over sodium sulphate and filtered. The residue was purified by column chromatography using hexane and ethyl acetate as eluent to obtain red solid with 25% yield.

^{1}H NMR (400MHz, $CDCl_3$) δ (ppm): 7.96 (s, 2 H), 7.72 (d, *J* = 8 Hz, 2 H), 7.65 (t, *J* = 8 Hz, 4 H), 7.54 (d, *J* = 8 Hz, 2 H), 7.01 (d, *J* = 4 Hz, 2 H), 6.58 (d, *J* = 4 Hz, 2 H).

Synthesis of *pp*-ADA (5):

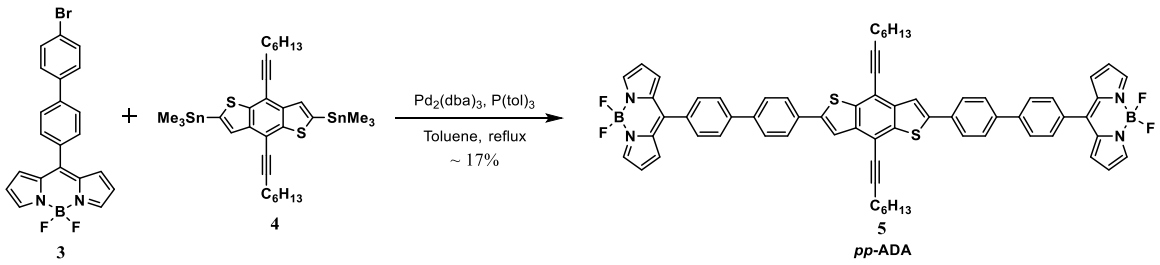

Scheme S5. Synthesis of ***pp*-ADA**.[S5]

Compound **4** (D_2) (50 mg, 0.068 mmol) and **3** (72 mg, 0.170 mmol) were dissolved in toluene and degassed by freeze-pump-thaw method. In a two-neck round bottomed flask,

Tris(dibenzylideneacetone)dipalladium(0) $Pd_2(dba)_3$, (2.1 mg, 0.0023 mmol), Tris(o-tolyl)phosphine $P(o\text{-}tol)_3$, (3.3 mg, 0.011 mmol) were taken and simultaneously compounds **3** and **4** were added and refluxed for 5 h. The reaction mixture was cooled and evaporated and purified by column chromatography by using $CHCl_3$ and hexane (80:20 of $CHCl_3$:hexane) to obtain a red solid with 17% yield.

^{1}H NMR (400MHz, $CDCl_3$) δ (ppm): 7.97 (s, 4 H), 7.91 (d, *J* = 8 Hz, 3 H), 7.86 (s, 1 H), 7.81 (d, *J* = 8 Hz, 4 H), 7.75 (d, *J* = 8 Hz, 4 H), 7.68 (t, *J* = 8 Hz, 4 H), 7.53 (d, *J* = 8 Hz, 1 H), 7.42 (d, *J* = 8 Hz, 1 H), 7.03 (s, 4 H), 6.58 (s, 4 H), 2.72 (t, *J* = 8 Hz, 4 H), 1.85-1.78 (m, 4 H), 1.29 (s, 12 H), 0.88 (s, 6 H).

^{13}C NMR (100 MHz, $CDCl_3$) δ (ppm): 146.95, 144.29, 144.10, 142.85, 140.20, 139.56, 139.18, 134.86, 134.07, 133.01, 131.52, 131.27, 127.63, 126.92, 119.09, 118.63, 114.09, 100.90, 37.11, 33.86, 31.95, 31.54, 31.49, 29.73, 29.39, 29.19, 28.97, 28.85, 28.76, 22.78, 22.72, 20.11, 14.23, 14.16.

^{11}B NMR (400 MHz, $CDCl_3$) δ (ppm): 0.54, 0.31, 0.09.

MS (HRMS-ESI): Calculated for **$C_{68}H_{56}B_2F_4N_4S_2Na$** $[M+Na]^+$: 1113.3966; found 1113.3252.

Synthesis of *pp*-AD (7):

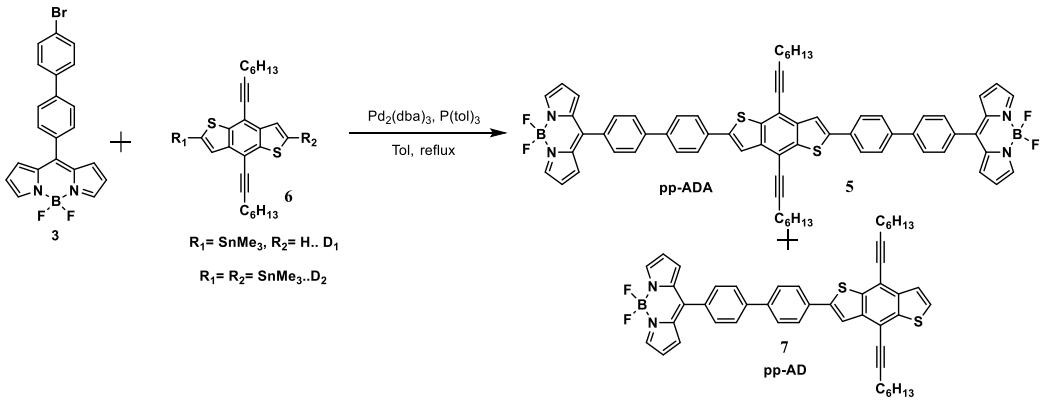

Scheme S6. Synthesis of ***pp*-AD**.[S5]

Compound **D_1+D_2** (50 mg, 0.068 mmol) and compound **3** (72 mg, 0.170 mmol) were dissolved in toluene and degassed by freeze-pump-thaw method. In a two-neck round bottomed flask, $Pd_2(dba)_3$ (2.1 mg, 0.002 mmol), $P(o\text{-}tol)_3$ (3.3 mg, 0.011 mmol) were taken and simultaneously compound **3** and **6** were added and refluxed for 5 h. The reaction mixture was cooled and evaporated and purified by column chromatography by using different percentage of $CHCl_3$ and hexane. ***pp*-ADA** was purified by column chromatography using 90:10 $CHCl_3$:hexane mixture and the mixture of Bodipy and ***pp*-AD** was obtained at 40:60 $CHCl_3$:hexane mixture followed by further purification using preparative TLC using 15:85 ethyl acetate:hexane as eluting solvent mixture with ~ 8 % yield.

^{1}H NMR for *pp*-AD (400MHz, $CDCl_3$) δ (ppm): 7.97 (s, 2 H), 7.93-7.81 (m, 2 H), 7.76 (d, *J* = 4 Hz, 1 H) 7.73-7.63 (m, 6 H), 7.55 (s, 2 H), 7.02 (d, *J* = 16 Hz, 2 H), 6.58 (s, 2 H), 2.89-2.54 (m, 4 H), 1.6 (s, 4 H), 1.43 (s, 8 H), 1.33 (s, 4 H), 0.96 (s, 6 H).

^{13}C NMR (100 MHz, $CDCl_3$) δ (ppm): 143.51, 139.43, 135.98, 134.91, 133.89, 133.82, 131.45, 131.39, 130.67, 129.87, 129.11, 128.99, 128.93, 128.55, 128.49, 128.43, 127.57, 125.53, 124.92, 114.21, 34.43, 33.97, 32.07, 31.57, 31.55, 31.09, 30.43, 29.84, 29.66, 29.51, 29.40, 29.30, 29.09, 28.78, 22.84, 14.28.

^{11}B NMR (400 MHz, $CDCl_3$) δ (ppm): 0.58, 0.35, 0.12.

MS (HRMS-ESI): Calculated for **$C_{47}H_{43}BF_2N_2S_2Na$** $[M+Na]^+$: 771.2826; found: 771.4825.

Synthesis of Me-*pp*-ADA (8):

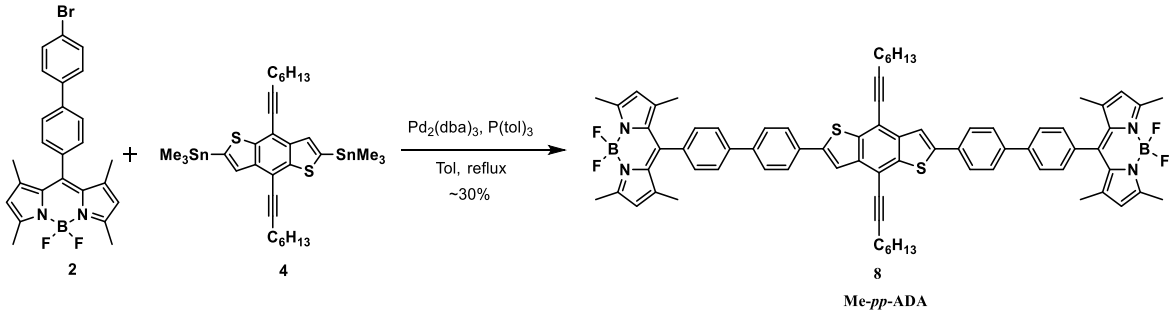

Scheme S7. Synthesis of **Me-*pp*-**ADA.[S5]

Compound **2** (50 mg, 0.104 mmol) and compound **4** (30 mg, 0.042 mmol) were taken in schlenk tube and degassed by freeze-pump-thaw method. In a two-neck round bottomed flask, $Pd_2(dba)_3$ (1.28 mg, 0.0014 mmol), $P(o\text{-}tol)_3$ (2.13 mg, 0.007 mmol) were taken and simultaneously compound **2** and **4** were added and refluxed for 5 h. The reaction mixture was cooled and evaporated and purified by column chromatography by using DCM and petroleum ether (percentage) to obtain the final compound as orange solid with 30% yield.

^{1}H NMR (400MHz, $CDCl_3$) δ (ppm): 7.91 (d, *J* = 12 Hz, 4 H), 7.86 (s, 2 H), 7.80-7.73 (m, 8 H), 7.71 (t, *J* = 8 Hz, 2 H), 7.39 (d, *J* = 8 Hz, 2 H), 6.01 (s, 4 H), 2.71 (t, *J* = 8 Hz, 4 H), 2.58 (t, *J* = 12 Hz, 12 H), 1.84-1.75 (m, 4 H), 1.47 (s, 12 H), 1.42 (m, 12 H), 0.87 (d, *J* = 8 Hz, 6 H).

^{13}C NMR (100 MHz, $CDCl_3$) δ (ppm): 143.13, 140.79, 139.32, 137.14, 135.86, 131.44, 130.95, 128.86, 128.67, 127.90, 127.45, 126.98, 124.80, 121.33, 121.29, 118.95, 114.09, 101.21, 33.87, 31.94, 31.45, 30.31, 30.19, 29.72, 29.62, 29.53, 29.46, 29.39, 29.27, 29.18, 29.09, 28.82, 25.93, 24.73, 22.71, 20.08, 14.65, 14.15.

^{11}B NMR (400 MHz, $CDCl_3$) δ (ppm): 1.07, 0.80, 0.55.

MS (HRMS-ESI): Calculated for **$C_{76}H_{73}B_2F_4N_4S_2$** $[M+H]^+$: 1203.5399; found: 1203.3386.

2. ^{1}H and ^{13}C NMR spectra

^{1}H NMR of *pp*-Biphenyl (1):

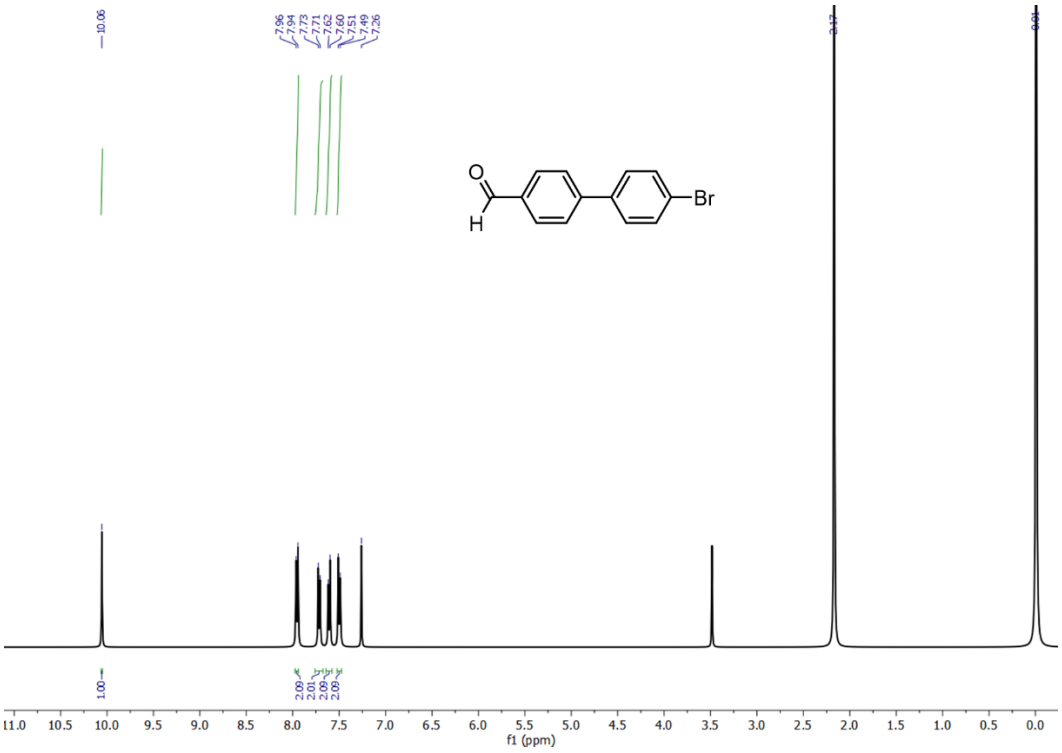

^{1}H NMR of Me *pp*-BODIPY (2):

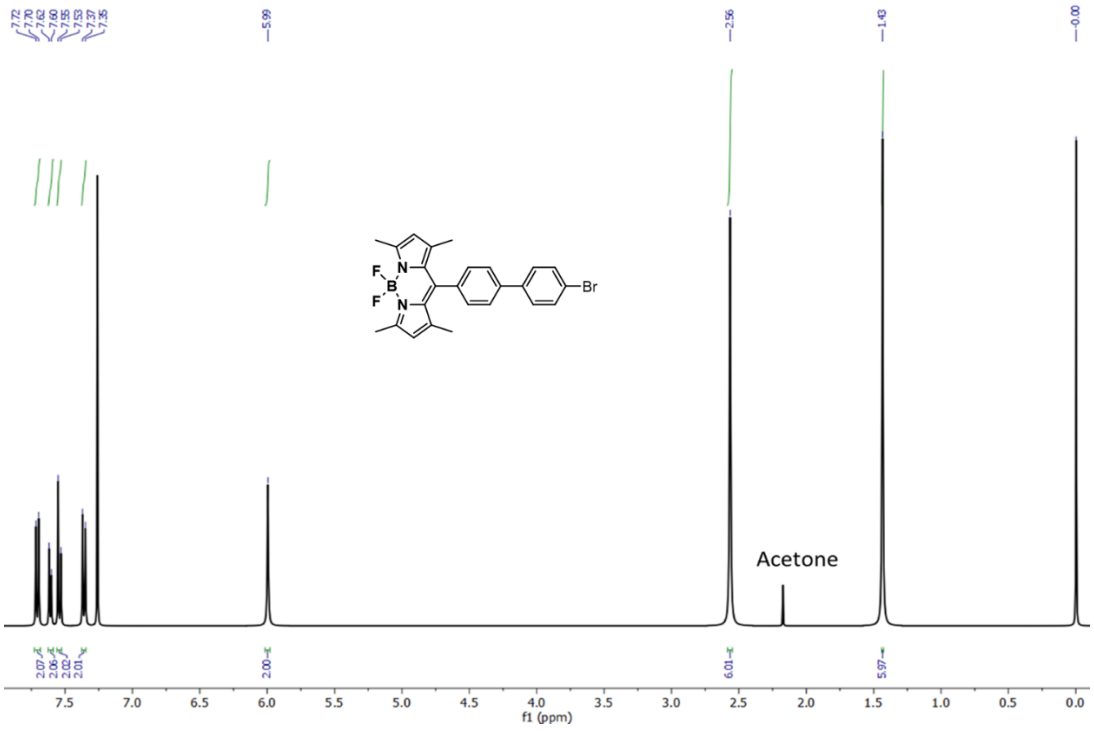

^{1}H NMR of *pp*-BODIPY (3):

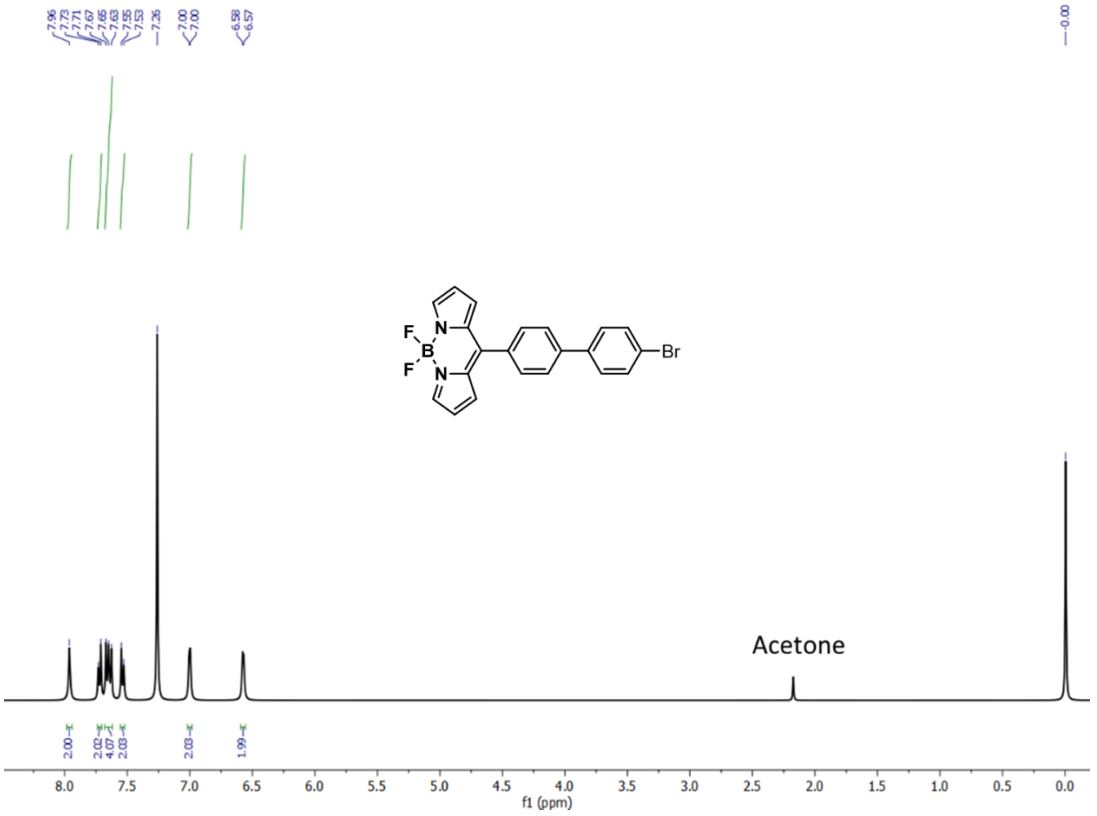

^{1}H NMR of *pp*-ADA (5):

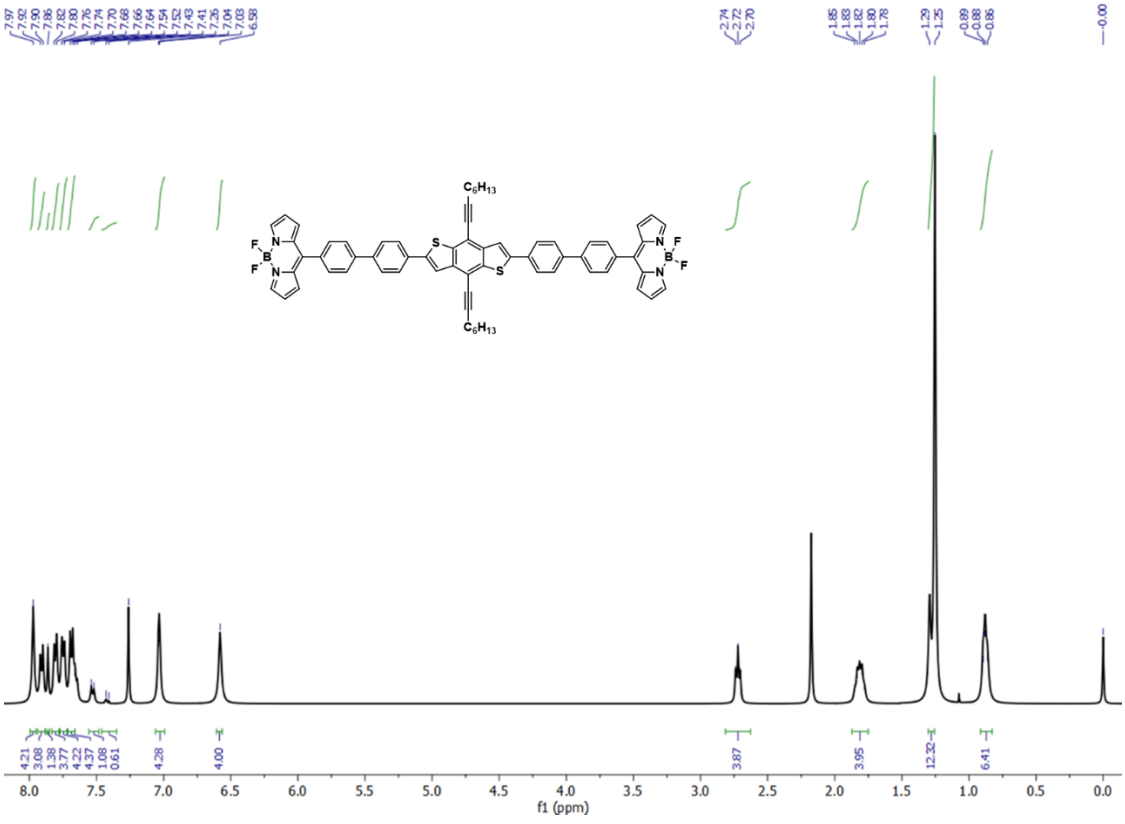

^{13}C NMR of *pp*-ADA (5):

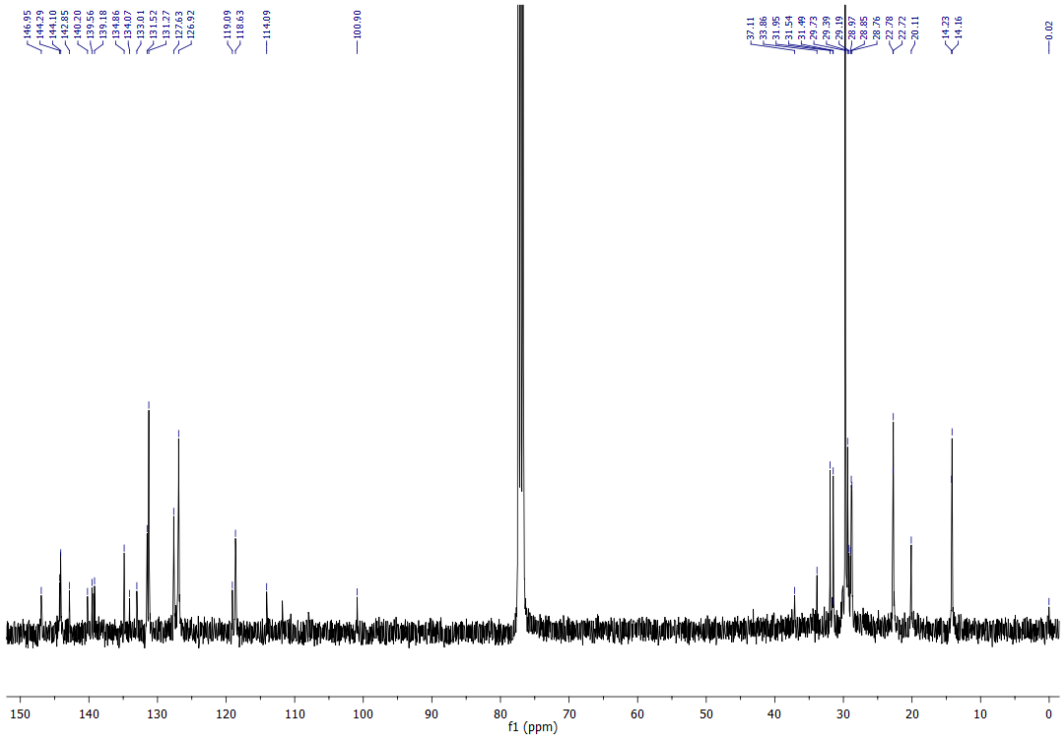

^{11}B NMR of *pp*-ADA (5):

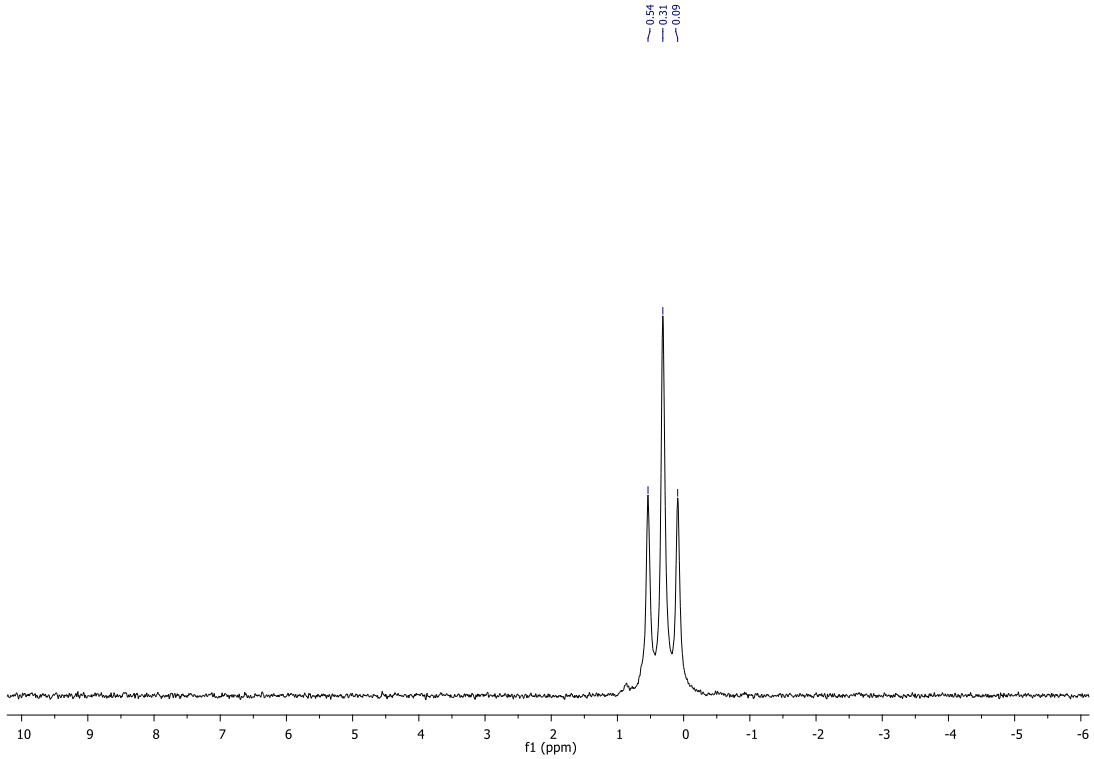

^{1}H NMR of *pp*-AD (7):

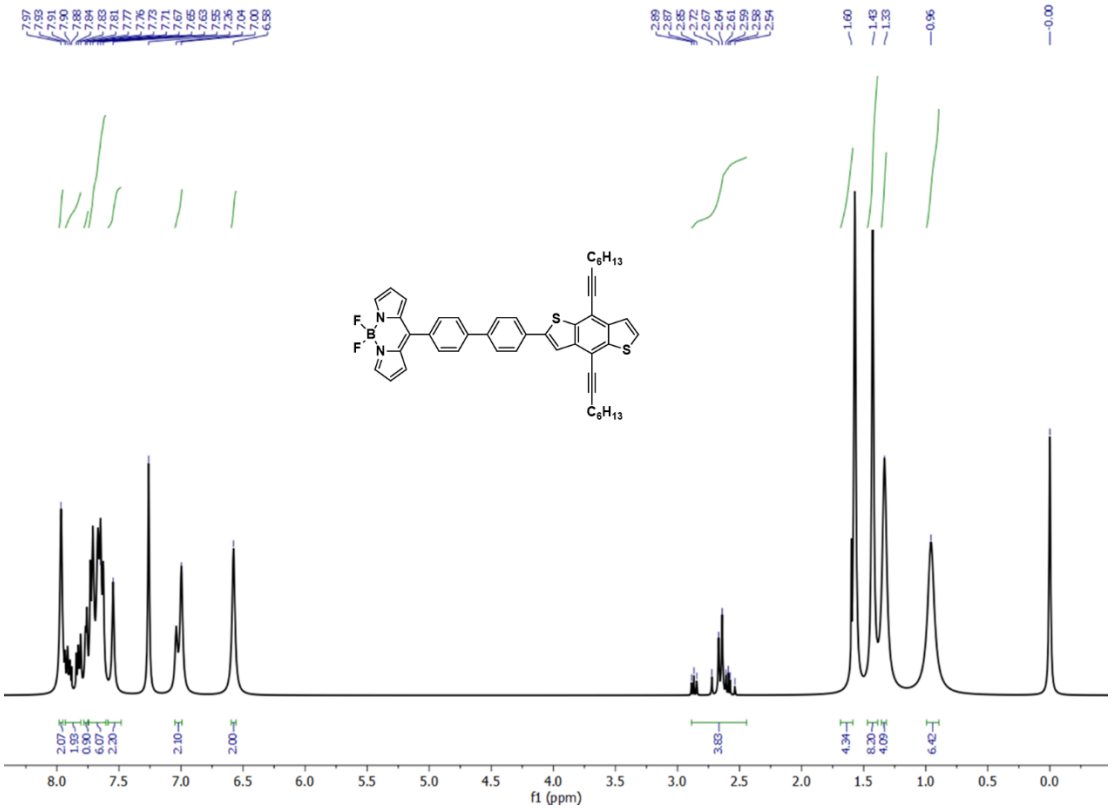

^{13}C NMR of *pp*-AD (7):

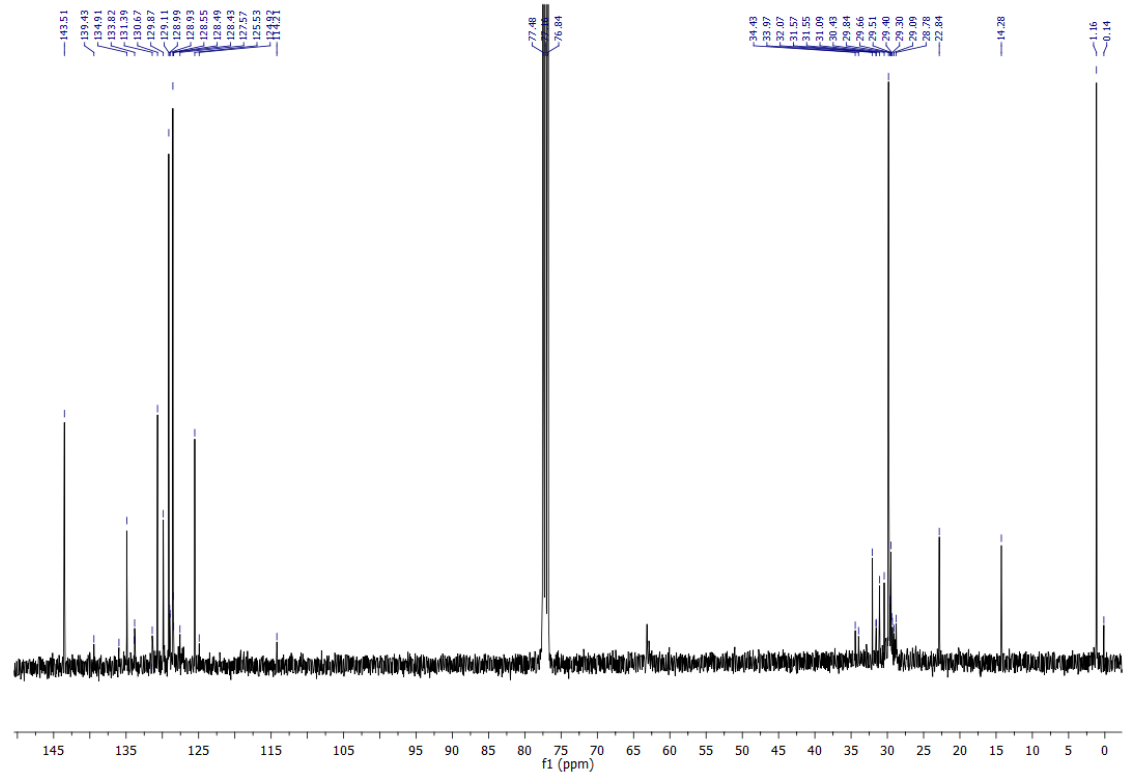

^{11}B NMR of *pp*-AD (7):

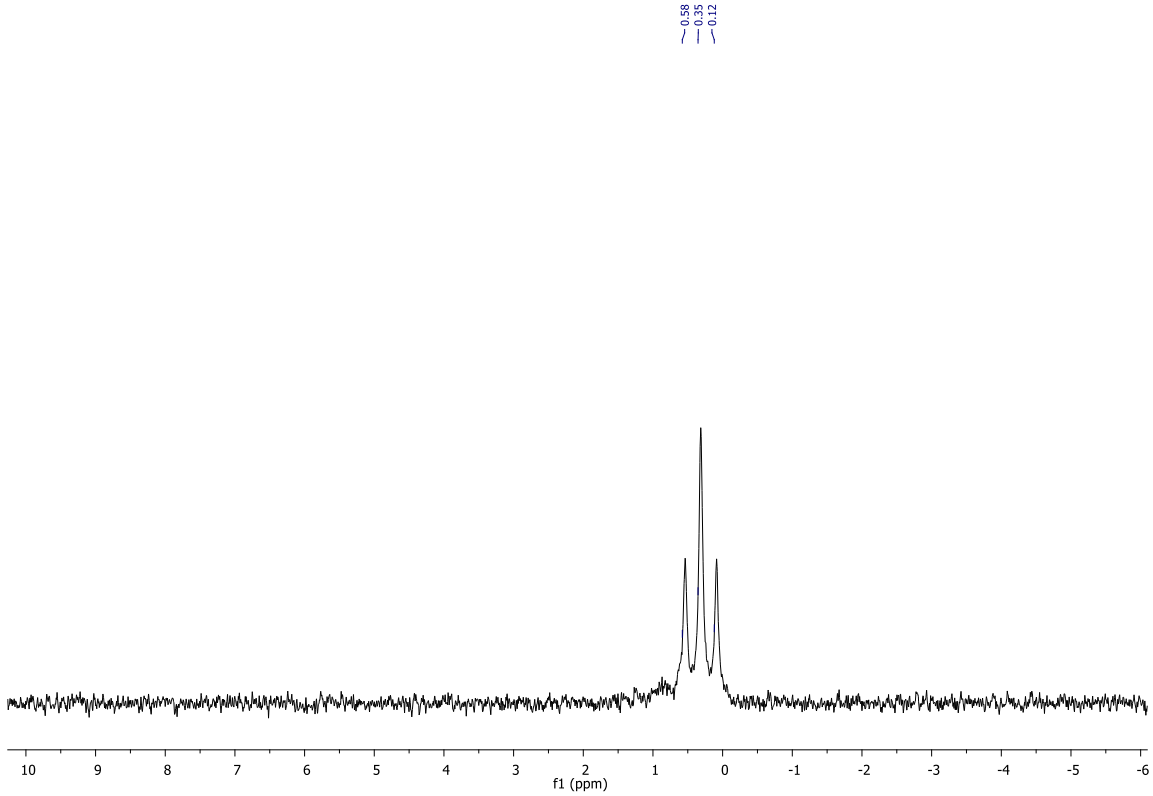

^{1}H NMR of Me-*pp*-ADA (8):

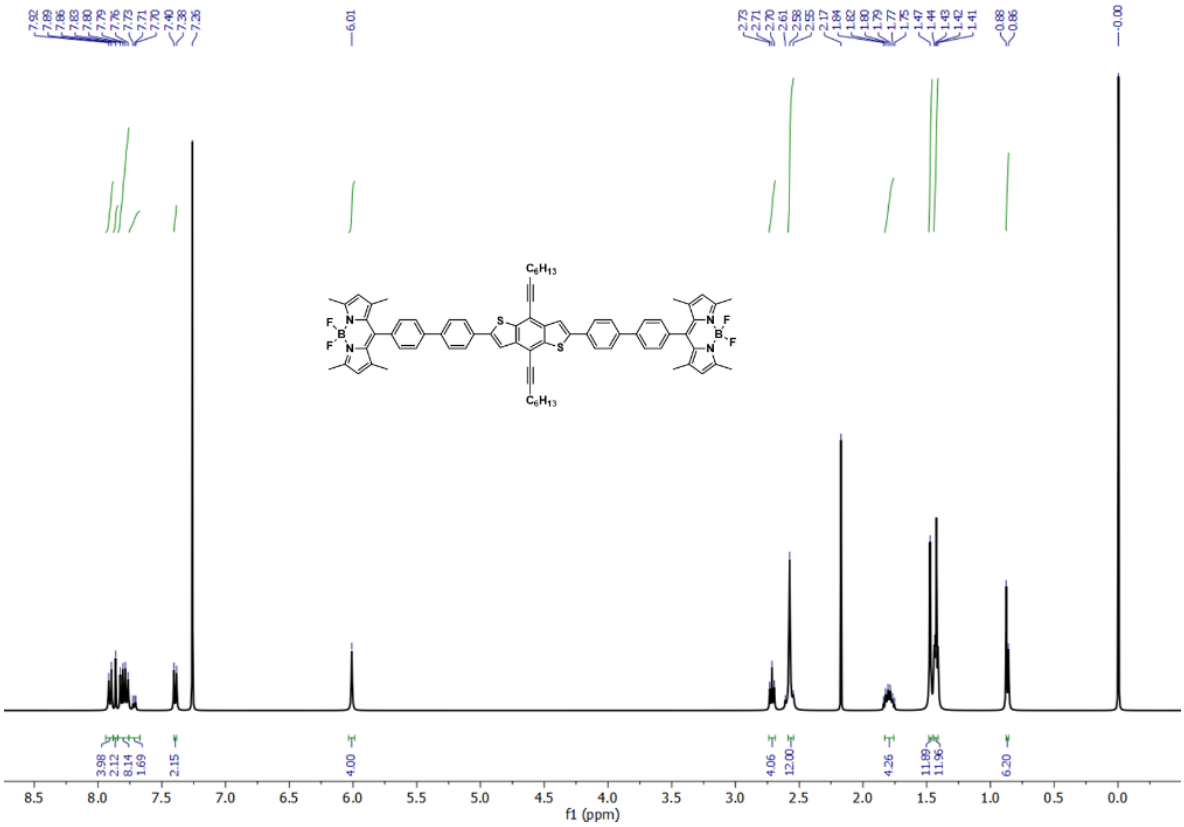

^{13}C NMR of Me-*pp*-ADA (8):

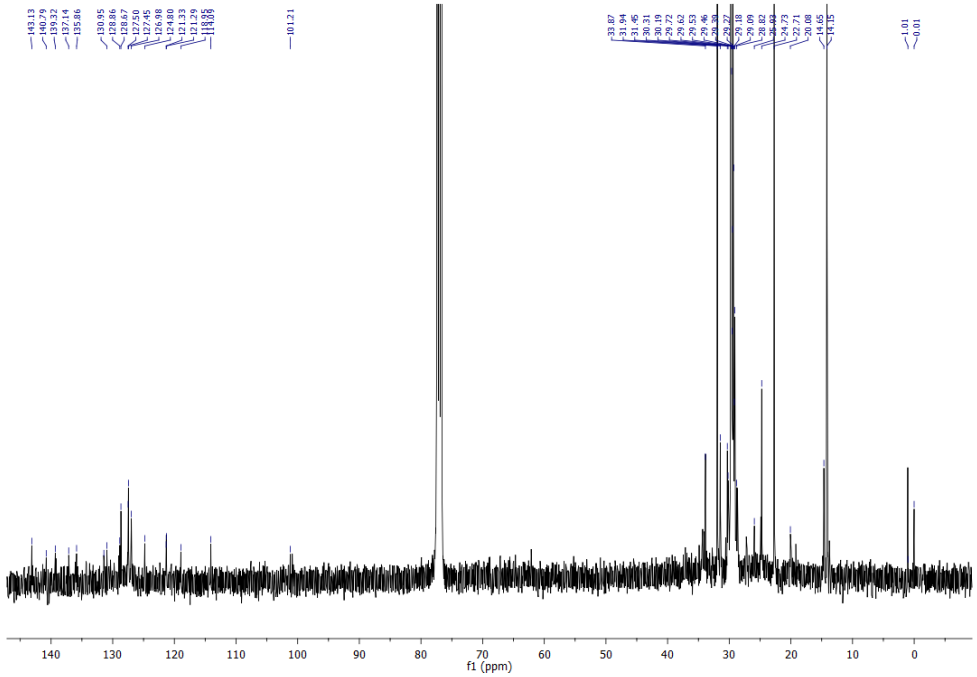

^{11}B NMR of Me-*pp*-ADA (8):

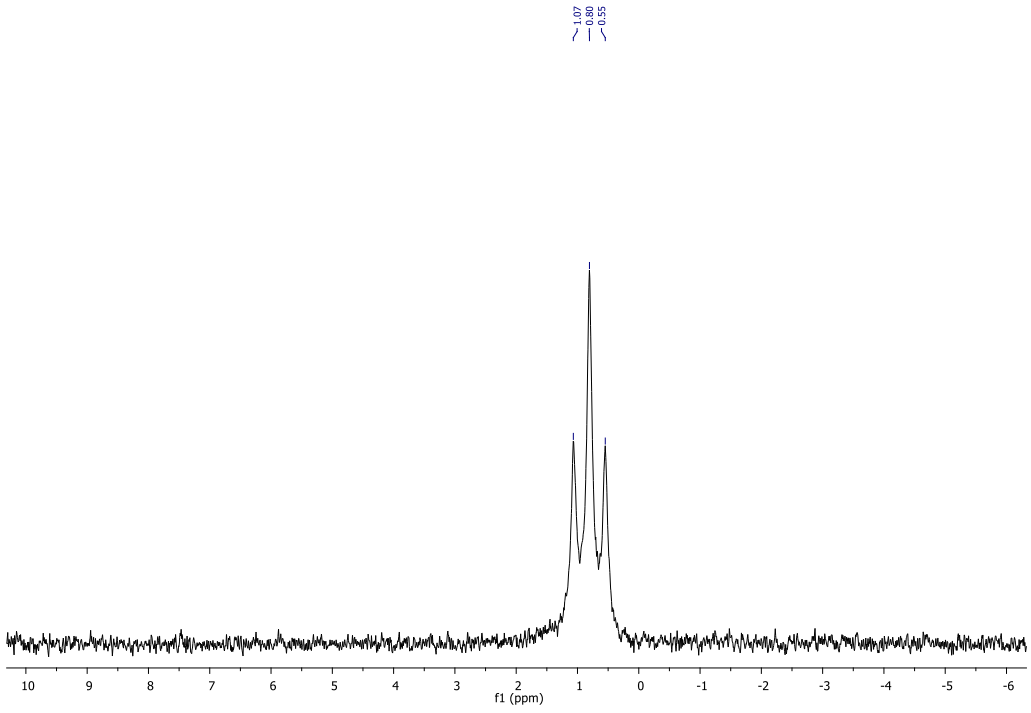

3. UV-Vis Absorption and Emission Spectra

UV/Vis absorption and fluorescence spectra of dyad ***pp*-AD** and triads ***pp*-ADA**, **Me-*pp*-ADA** were measured in chloroform ($CHCl_3$) at c ~ 10^{-6} M. Three major peaks (312-322 nm, 360-390 nm and 504 nm) were obtained for all compounds. Upon excitation of ***pp*-AD** and ***pp*-ADA** at 391 nm, the emission spectra were dominated by a strong emission from the BDT (430 nm) that supresses the very weak emission from BODIPY (524 nm) and TICT (725 nm) and thus these two bands are barely visible (Fig. S1 g, h, i). However, when ***pp*-ADA** was excited at the BODIPY abs. (504 nm), significant emission bands are observed due to the BODIPY (524 nm) and the TICT (725 nm) as shown in Fig. S1 (d, e).

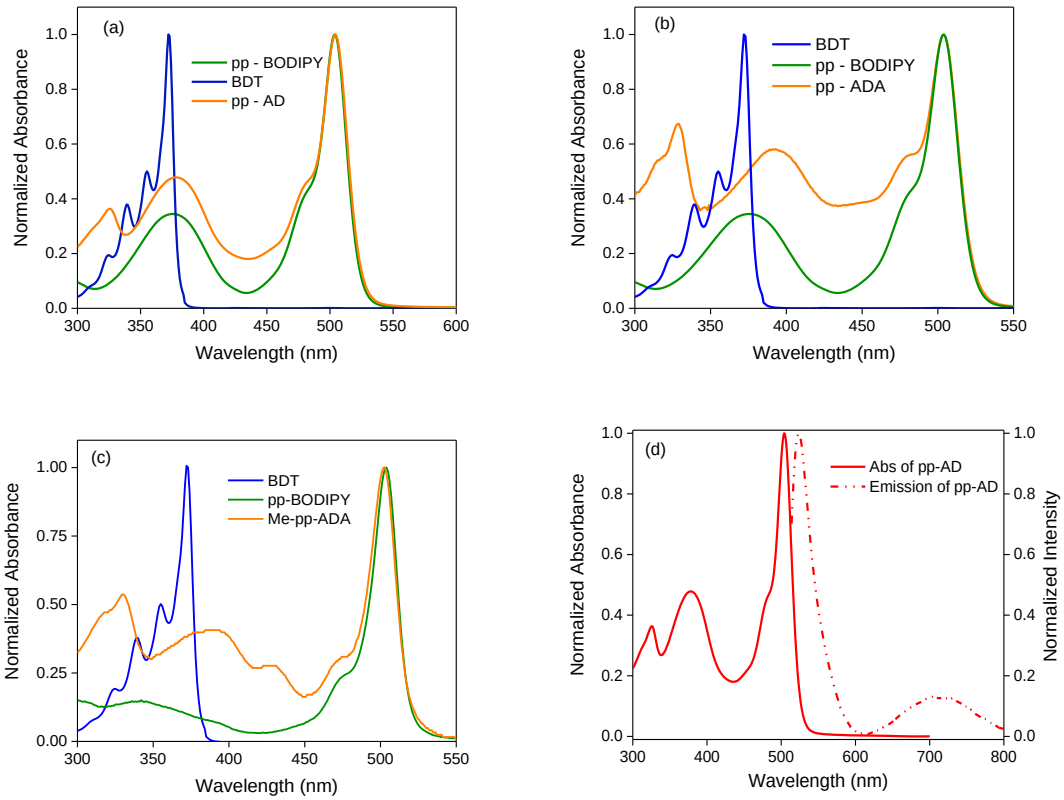

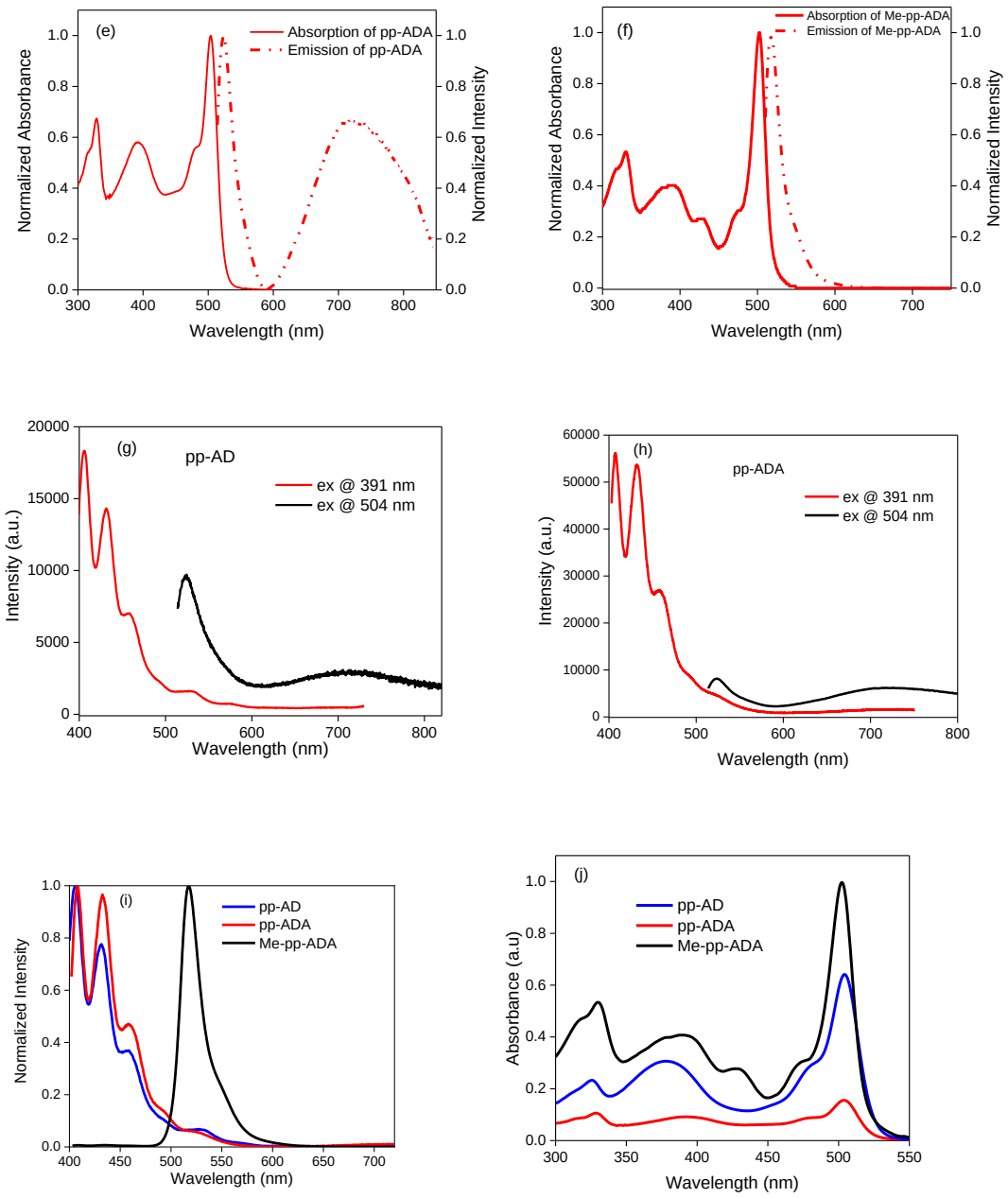

Figure S1. UV/Vis absorption of : (a) ***pp*-AD**, (b) ***pp*-ADA** and (c) **Me-*pp*-ADA** along with their donor and acceptor counterparts and fluorescence spectra of : (d) ***pp*-AD**, (e) ***pp*-ADA** and (f) **Me-*pp*-ADA** with their absorption spectra excited at 504 nm (***pp*-AD**), 504 nm (***pp*-ADA**) and 502 nm (**Me-*pp*-ADA**) in $CHCl_3$; emission spectra of (g) ***pp*-AD** and (h) ***pp*-ADA** excited at donor (391 nm) as well as BODIPY (504) absorption; (i) emission spectra of ***pp*-AD**, ***pp*-ADA** and **Me-*pp*-ADA** excited at 391 nm; (j) absorption spectra (not normalized) of ***pp*-AD**, ***pp*-ADA** and **Me-*pp*-ADA**.

4. Solvatochromism

Since both rotors ***pp*-AD** and ***pp*-ADA** showed TICT emission, fluorescence solvatochromism study was performed in solvents of different polarities. In non-polar solvents such as methyl

cyclohexane (MCH) and toluene, ***pp*-AD** and ***pp*-ADA** showed only a peak corresponding to BODIPY emission. In TICT rotors, since the excited state show higher dipole moment than their ground state, they are preferentially stabilized by polar solvents than their respective ground states.[S6] Accordingly, increasing solvent polarity leads to bathochromic shift in the emission profile of these rotors. In polar solvents such as chloroform ($CHCl_3$), tetrahydrofuran (THF) and 2-methyltetrahydrofuran (2-MeTHF), ***pp*-AD** and ***pp*-ADA** showed dual emission and the longer wavelength TICT band shifted bathochromically in more polar solvents (Figure S2). In dichloromethane (DCM), the TICT state was not observed for any of the rotors (***pp*-AD** and ***pp*-ADA**) presumably due to rapid non-radiative deactivation. Furthermore, solvatochromic study was performed for both the rotors in a binary mixture of polar and non- polar (THF/Hexane) solvents. For ***pp*-ADA**, as the percentage of hexane was increased from 0 to 50 % (v/v), the TICT band was hypsochromically shifted and intensity increased due to increase in hydrophobicity of the solvent mixture which renders the ***pp*-ADA** less twisted. Upon further increasing hexane percentage to 60 % and 80 % (v/v), the intensity decreased with peak while the LE emission became the prevailing peak (Figure S3). At 90 % hexane, only LE emission was observed and no TICT peak was observed. Thus, for ***pp*-ADA**, the prominent hypsochromic shift was observed from 720 nm to 522 nm and the TICT band disappeared with concomitant emergence of the LE band as a shoulder upon increasing hexane percentage from 0 % to 90 %. Similarly, ***pp*-AD**, hypsochomic shift was observed from 724 nm to 521 nm upon increasing hexane percentage from 0 % to 90 % (Figure S3). Thus, hyposchromic shift upon decreasing solvent polarity confirmed the TICT states in ***pp*-AD** and ***pp*-ADA**.

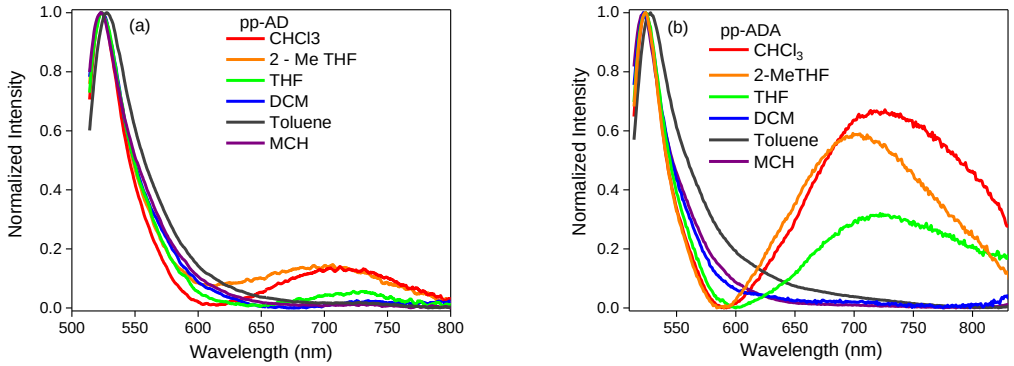

Figure S2. Emission of (a) ***pp*-AD** and (b) ***pp*-ADA** excited at 504 nm in solvent of different polarity.

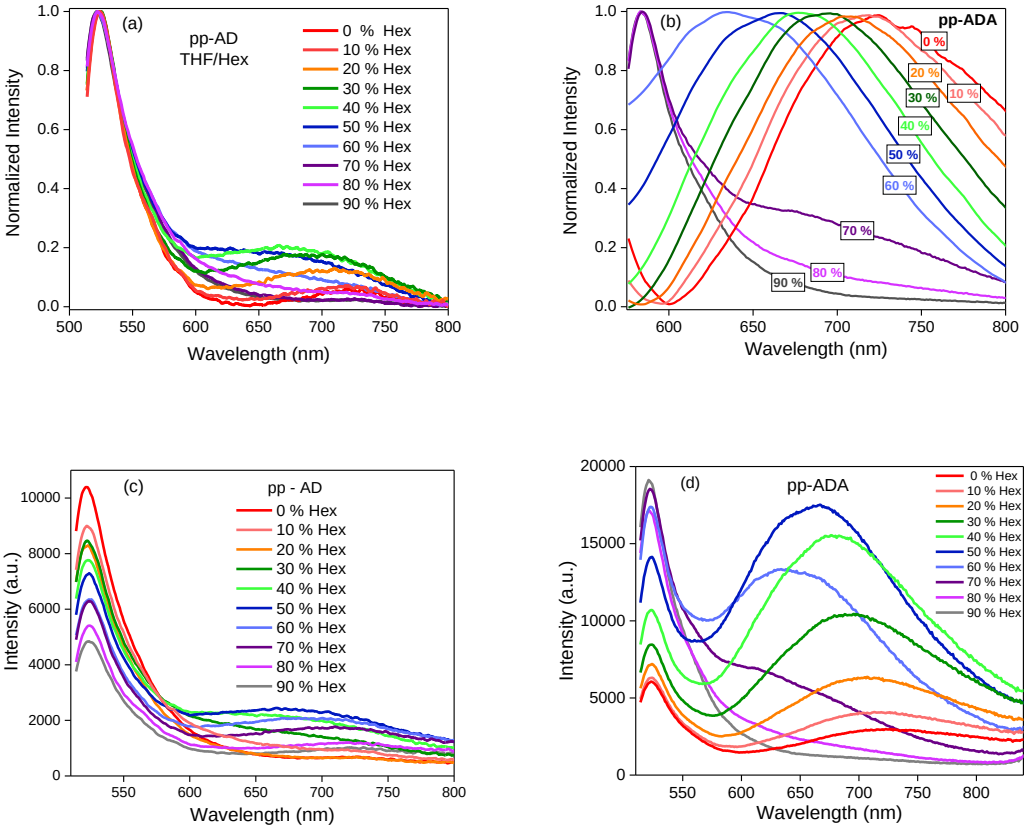

Figure S3. Normalized emission of (a) ***pp*-AD**, (b) ***pp*-ADA** and unnormalized emission of (c) ***pp*-AD**, (d) ***pp*-ADA** in different percentage of THF/Hexane and (inside the box, 0 %, 10 % to 90 % indicate the percentage of hexane in THF solutions).

UV/Vis absorption and emission spectra of ***pp*-ADA** and **Me-*pp*-ADA** was also performed in thin film (Fig S4a and b). In UV/Vis absorption spectra of ***pp*-ADA**, three major red shifted (335 nm, 420 nm and 542 nm) peaks were observed as compared to spectra in solution.

Similarly, in **Me-*pp*-ADA** three major peaks (338 nm, 400 nm and 512 nm) were obtained. In ***pp*-ADA**, upon excitation at 542 nm, a minor peak at 561 nm and a major peak at 736 nm was observed while in **Me-*pp*-ADA**, upon excitation at 512 nm three peaks around 531 nm, 555 nm and 640 nm were observed. Drop casted films of ***pp*-ADA** showed fluorescence thermochromism i.e. change in colour by varying temperature as shown in figure S4 (c). Interestingly, red emission was observed (~ 732 nm) in solid compound for ***pp*-ADA** and mechanochromism study of ***pp*-ADA** showed no shift in emission spectra before and after grinding of solid sample as shown in Fig. S4(d).

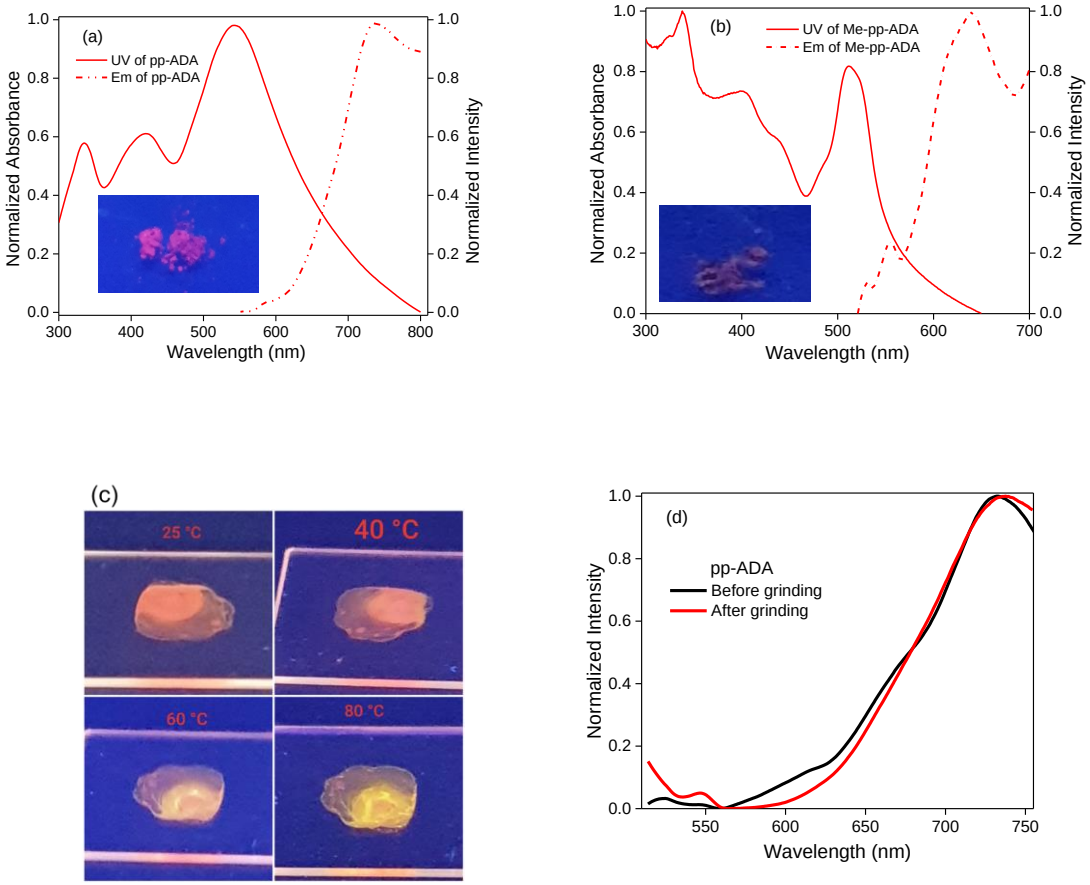

Figure S4. UV/Vis and emission of (a) ***pp*-ADA** and (b) **Me-*pp*-ADA** in thin film. Inset in figure (a, b) picture of solid compound of ***pp*-ADA** and **Me-*pp*-ADA** and (c) Drop casted films of ***pp*-ADA** on quartz substrates at different temperatures, inside UV chamber under 365 nm UV light. (d) Emission spectra of solid compound of ***pp*-ADA** before and after grinding.

5. Cyclic Voltammetry

Cyclic voltammetry (CV) measurements were performed for ***pp*-AD**, ***pp*-ADA** and **Me-*pp*-ADA** as well acceptor subunits ***pp*-BODIPY** and **Me-*pp*-BODIPY** and donor subunit BDT in dry DCM with 0.1 M tetrabutylammonium hexafluophosphate as supporting electrolyte and Ag/AgCl as reference electrode to determine the HOMO and LUMO energy levels. Internal calibration was performed by ferrocene prior to all measurements. Based on the first oxidation potential onset (E_{ox}^{onset}) and first reduction potential onset (E_{red}^{onset}), the HOMO and LUMO levels were calculated according to the relation: [S7]

HOMO $= -(E_{ox}^{onset} + 4.76)$ eV and

LUMO $= -(E_{red}^{onset} + 4.76)$ eV.

The cyclic voltammograms are presented in figure S5 and calculation of HOMO, LUMO energy levels are presented in table S1. For model compounds ***pp*-BODIPY** & BDT, the optical gap (E_g) were calculated as E_g (eV) = $1241/\lambda_{onset}$, where λ_{onset} is the absorption onset values obtained from UV/Vis absorption spectra and the HOMO and LUMO were calculated using the above equations and the E_g value. Accordingly, calculated HOMO energies for ***pp*-BODIPY**, **Me-*pp*-BODIPY** and BDT were - 6.48 eV, -5.93 eV and − 5.98 eV and LUMO energies were – 4.14 eV, - 4.06 eV and - 2.74 eV respectively. For the dyad ***pp*-AD** and triads ***pp*-ADA**, **Me-*pp*-ADA** both oxidation and reduction peaks are observed that resemble the oxidation peaks of BDT and reduction peaks of BODIPY. This observation is indicative of the fact that there is no significant interaction of the donor (D) and acceptor (A) in the ground states in all the molecules and the D and A retain their individual optical and redox properties. From the first oxidation onset, HOMO levels were calculated for ***pp*-AD**, ***pp*-ADA** and **Me-*pp*-ADA** as - 5.93 eV, - 5.87 eV and - 5.27 eV while the LUMO energies calculated

from first reduction onset were - 4.04 eV, - 4.19 eV and – 3.88 eV respectively.

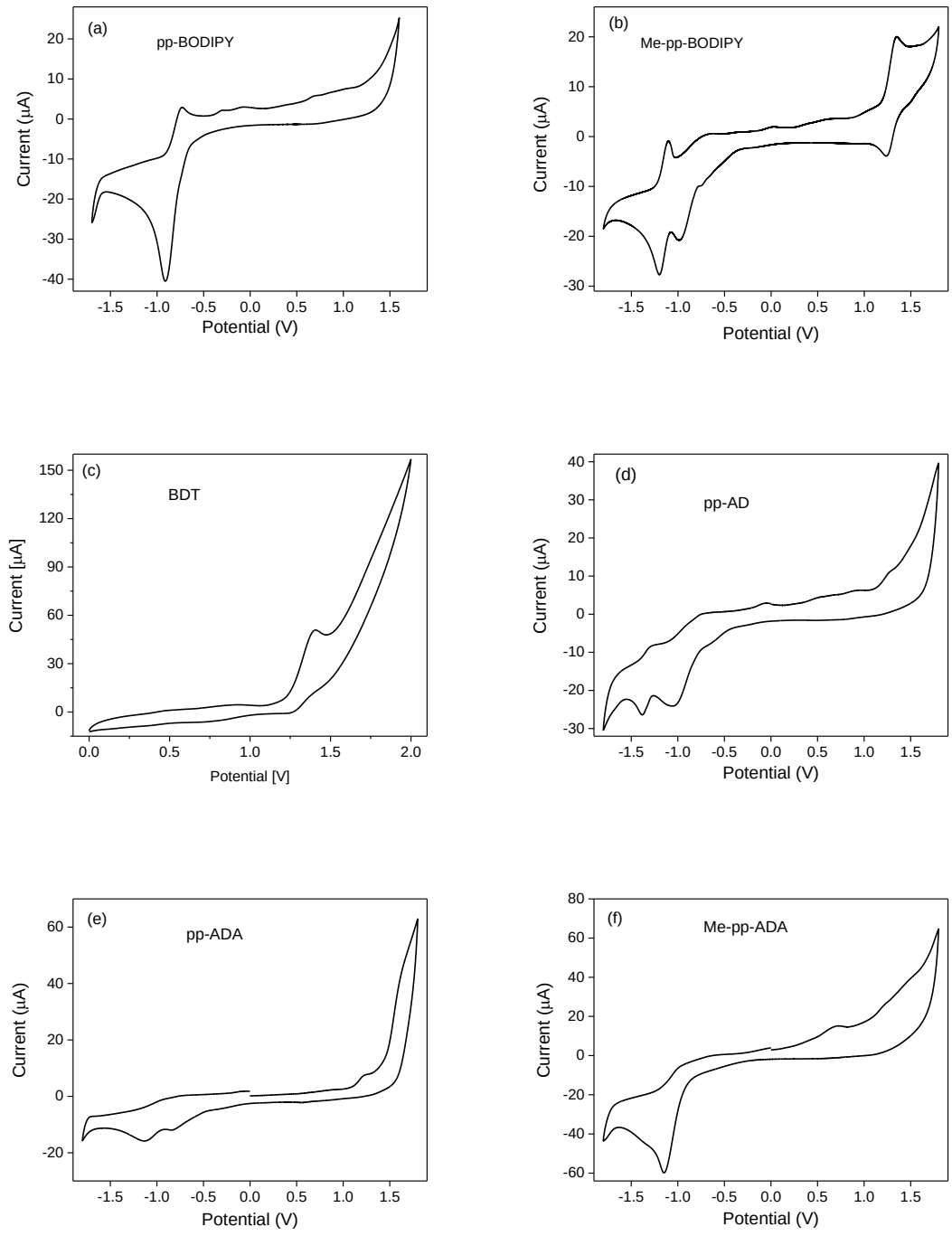

Figure S5. Cyclic voltammogram of (a) ***pp*-BODIPY**, (b) **Me-*pp*-BODIPY**, (c) **BDT** (d) ***pp*-AD**, (e) ***pp*-ADA**, (f) **Me-*pp*-ADA** in dry dichloromethane with 0.1 M tetrabutylammonium hexafluorophosphate ($TBAHPF_6$) and potentials measured vs Ag/AgCl reference electrode.

Table S1: Redox and optical properties of subchromophores donor BDT and acceptors ***pp*-BODIPY**, **Me-*pp*-BODIPY**, dyad ***pp*-AD** and triads ***pp*-ADA** and **Me-*pp*-ADA** based on cyclic voltammetry.

Compound	E_{ox}^{onset} (V)	HOMO (eV)	E_{red}^{onset} (V)	LUMO (eV)	$^{a}\lambda_{onset}$ (nm)	E_g (eV)	Molar extinction coefficient (ε) ($M^{-1}cm^{-1}$)
***pp*-BODIPY**	-	- 6.48	- 0.615	- 4.14	530	2.34	-
Me-*pp*-BODIPY	1.169	- 5.93	- 0.695	- 4.06	-	1.87	-
BDT[S1]	1.22	- 5.98	-	- 2.74[b]	383	3.23	-
***pp*-AD**	1.17	- 5.93	- 0.72	- 4.04	-	1.89	27370
***pp*-ADA**	1.11	- 5.87	- 0.57	- 4.19	-	1.68	36280
Me-*pp*-ADA	0.96	- 5.72	- 0.88	- 3.88	-	1.84	31758

[a] absorption onset obtained from UV/Vis absorption spectra. [b]Calculated from difference of HOMO and E_g

6. DFT Calculations

Table S2. FMO energy levels of compounds ***pp*-AD**, ***pp*-ADA** and **Me-*pp*-ADA** calculated by B3LYP/6-31G(d,p).

Compound	HOMO-1 (eV)	HOMO (eV)	LUMO (eV)	LUMO+1 (eV)
***pp*-AD**	-5.86	-5.23	-2.80	-1.90
***pp*-ADA**	-5.90	-5.28	-2.85	-2.83
Me-*pp*-ADA	-5.36	-5.22	-2.36	-2.36

Table S3. FMO composition analysis for ***pp*-AD**, ***pp*-ADA** and **Me-*pp*-ADA**.

Compound	Orbital No.	MO	Energy (eV)	Contribution from BDT donor (%)	Contribution from BODIPY acceptor (%)	Contribution from biphenyl spacer (%)
***pp*-ADA**	247	LUMO+1	-2.83	0	88	11
	246	**LUMO**	**-2.85**	**2**	**85**	**13**
	245	**HOMO**	**-5.29**	**86**	**0**	**14**
	244	HOMO-1	-5.90	0	99	1
***pp*-AD**	159	LUMO+1	-1.66	72	2	26
	158	**LUMO**	**-2.71**	**0**	**92**	**8**
	157	**HOMO**	**-5.3**	**97**	**0**	**3**
	156	HOMO-1	-5.87	0	99	1

Me-*pp*-ADA	279	LUMO+1	-2.37	0	98	2
	278	**LUMO**	**-2.37**	**0**	**97**	**2**
	277	**HOMO**	**-5.22**	**85**	**0**	**15**
	276	HOMO-1	-5.36	0	100	0

7. Fluorescence Quantum Yield

Fluorescence quantum yield was measured by using relative method using Rhodamine B (Φ_R = 0.5) in ethanol as reference dyes and using the following equation: [S8]

$$\Phi = \Phi_R\,(I/I_R)\,(A_R/A)\,(\lambda_{exR}/\lambda_{ex})\,(n^2/n^2_R)$$

where Φ_R is the quantum yield of reference dye Rhodamine B in ethanol, I and I_R are integrated fluorescence intensities of compounds and reference dye respectively, A and A_R are the absorbance of the compounds and reference dye respectively, and n and n_R are the refractive indices of solvent(s) used for compounds and reference respectively. The compounds ***pp*-AD**, ***pp*-ADA** and **Me-*pp*-ADA** were dissolved in $CHCl_3$ in three different concentrations (c ~ 10^{-5}-10^{-6} M) such that their absorbance was less than or equal to 0.1 and their absorption and fluorescence spectra were recorded (at excitation wavelengths of 504 nm, 504 nm, 393 nm for ***pp*-AD**, ***pp*-ADA** and **Me-*pp*-ADA** respectively). Absorbance and fluorescence spectra were recorded for three different concentrations of Rhodamine B (excitation wavelength of 543 nm) in ethanol (c ~ 10^{-5}-10^{-6} M). Fluorescence quantum yields were then calculated using the above equation for each compound.

Table S4: Relative quantum yields of triads ***pp*-AD**, ***pp*-ADA** and **Me-*pp*-ADA** by using comparative method and Rhodamine B as a reference dye.

Compound	**Absorbance**			**Integrated Fluorescence Intensity**			**Quantum Yield $\Phi=\Phi_R(I/I_R)(A_R/A)(\lambda_{exR}/\lambda_{ex})(n^2/n^2_R)$**	
	1	**2**	**3**	**1**	**2**	**3**	**Φ_i**	**Φ_{avg}**
***pp*-AD**	0.0104	0.0181	0.0261	46789.6	84448.1	137538.5	0.031	

							0.034 0.038	0.034
***pp*-ADA**	0.0261	0.0504	0.0658	103785.1	186475.7	151326.8	0.028 0.024 0.021	0.024
Me-*pp*-ADA	0.0504	0.0804	0.1001	61959.5	83432.3	168432	0.200 0.220 0.200	0.206
Rhodamine B (ethanol)	0.0146	0.0169	0.0188	13388573.1	1374809.6	1667805	0.5 (reported value)[S9]	

8. Excitation Energy Transfer in Me-pp-ADA

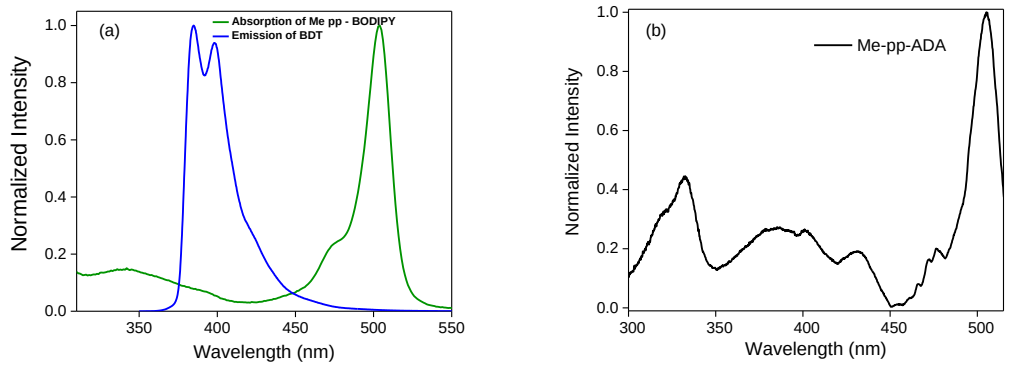

Figure S6. (a) Emission of BDT and absorption of BODIPY showing a weak spectral overlap; (b) fluorescence excitation spectrum of **Me-*pp*-ADA** recorded at BODIPY emission at 516 nm.

The energy transfer efficiency (ETE) of **Me-*pp*-ADA** (ETE) can be measured by using the following equation[S10]

$$ETE = 1 - \Phi_{DA}/\Phi_{D}$$

where Φ_{DA} is the quantum yield of BDT in triad **Me-*pp*-ADA** and Φ_{D} is the quantum yield of free BDT. Absorbance and fluorescence spectra were recorded for three concentrations of BDT (excitation wavelength of 355 nm) and BDT of **Me-*pp*-ADA** (excitation wavelength of

391 nm) in THF solution and the quantum yield was subsequently calculated as explained above by using Anthracene in ethanol as reference dye and the values are tabulated in table S5. Accordingly, a quantum yield Φ_{DA} of ~ 0.021 for the BDT in **Me-*pp*-ADA** and Φ_D of ~ 0.17 for free donor BDT led to an ETE for **Me-*pp*-ADA** of ~ 88 % indicating an efficient excitation energy transfer from BDT to BODIPY.

Table S5: Relative quantum yields of BDT and donor part of **Me-pp-ADA** by using comparative method and Anthracene as a reference dye.

Compound	**Absorbance**			**Integrated Fluorescence Intensity**			**Quantum Yield $\Phi=\Phi_R(I/I_R)(A_R/A)(\lambda_{exR}/\lambda_{ex})(n^2/n^2_R)$**	
	1	**2**	**3**	**1**	**2**	**3**	**Φ_i**	**Φ_{avg}**
BDT	0.0395	0.0604	0.0799	28152562.3	31585520	36884900	0.223 0.16 0.13	0.17
Donor part of Me-PP-ADA	0.0043	0.0131	0.0151	407004.2	1007515.9	915474.1	0.027 0.021 0.016	0.021
Anthracene (ethanol)	0.0414	0.0659	0.0809	38066300	62617500	79902400	0.27 (reported value)	

AIE emission of ***pp*-AD** and ***pp*-ADA** using Internationale de l'Eclairage (CIE) coordinates showed prominent colour change from green (CIE coordinates of 0.36,0.61) to orange (CIE coordinates of 0.47,0.51) for ***pp*-AD** and from green (0.39,0.58) to orange (0.52,0.46) for ***pp*-ADA** by gradually increasing the water percentage in THF solutions.

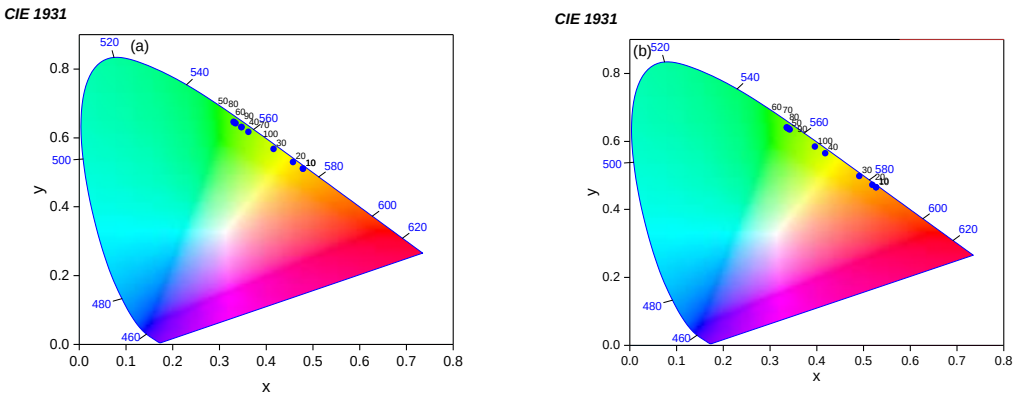

Figure S7. CIE Chromaticity plot of (a) ***pp*-AD** and (b) ***pp*-ADA** in water/THF mixture (numbers in black indicate the volume percentage of THF added in water).

UV/Vis Absorption Spectra in Water and THF Mixture

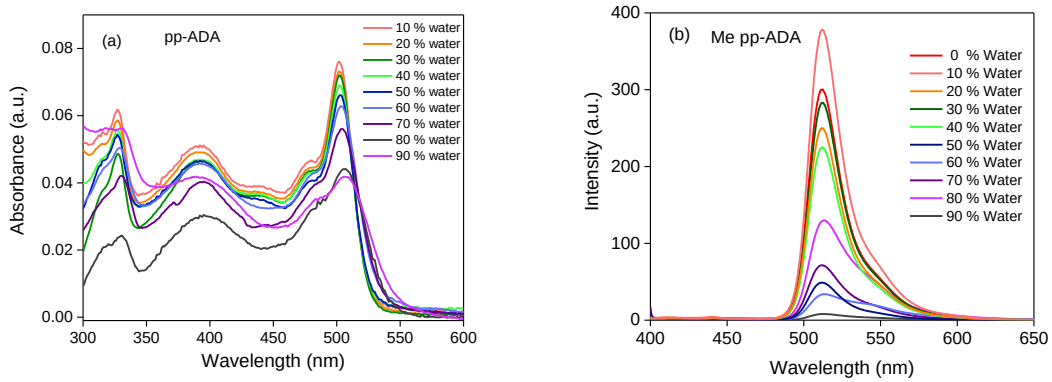

Figure S8. (a) UV/Vis absorption spectra of ***pp*-ADA** and (b) emission spectra of **Me-*pp*-ADA** in different percentage of THF and water.

9. Temperature Dependent Emission Spectra & Ratiometric Temperature Sensing

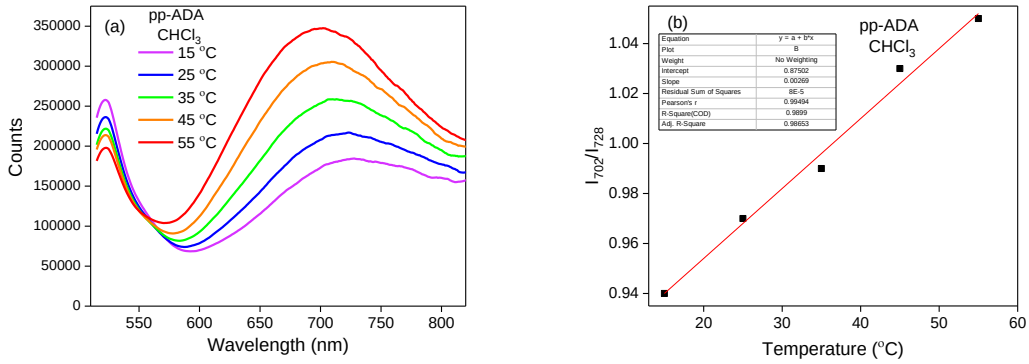

Figure S9. (a) Temperature dependent emission spectra of ***pp*-ADA** and b) Emission intensity ratio (I_{702}/I_{728}) with best fit equation at different temperature for ***pp*-ADA** in $CHCl_3$. The intensities I_{728} and I_{702} indicate the emission intensities at the initial temperature (15 °C) and final temperature (55 °C).[S11]

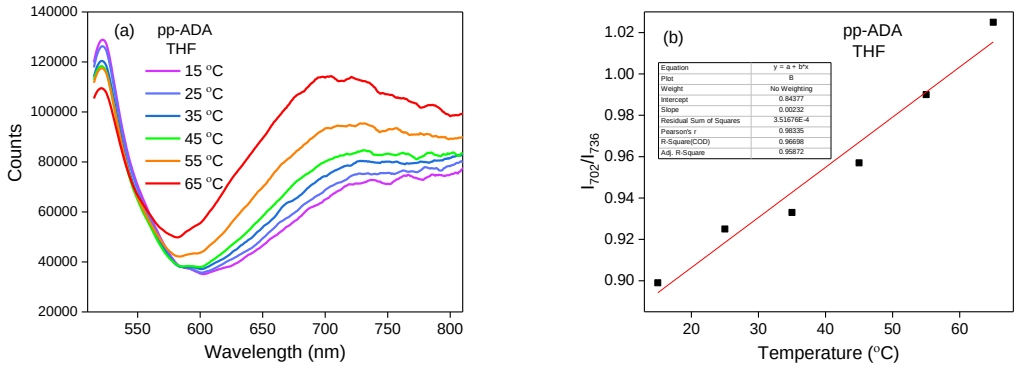

Figure S10. (a) Temperature dependent emission spectra of ***pp*-ADA** and b) Emission intensity ratio (I_{702}/I_{736}) with best fit equation at different temperature for ***pp*-ADA** in THF. The intensities I_{736} and I_{702} indicate the emission intensities at the initial temperature (15 °C) and final temperature (55 °C).

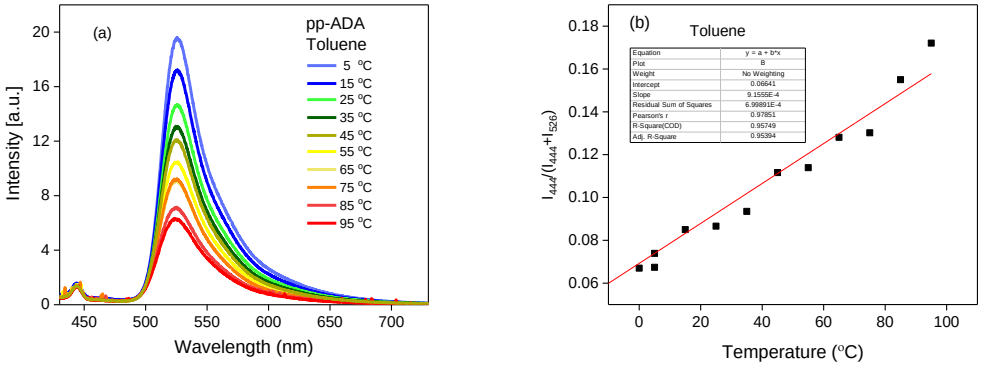

Figure S11. (a) Temperature dependent emission spectra of ***pp*-ADA** in toluene and (b) Emission intensity ratio with best fit equation at different temperature for ***pp*-ADA** in Toluene.

For ***pp*-AD** and ***pp*-ADA** in toluene however, only one peak due to LE state was observed and temperature variation from 5 °C to 95 °C led to the decrease of the LE emission intensity attributed to enhanced molecular motions upon increasing temperature leading to non-radiative deactivation (Figure S11).

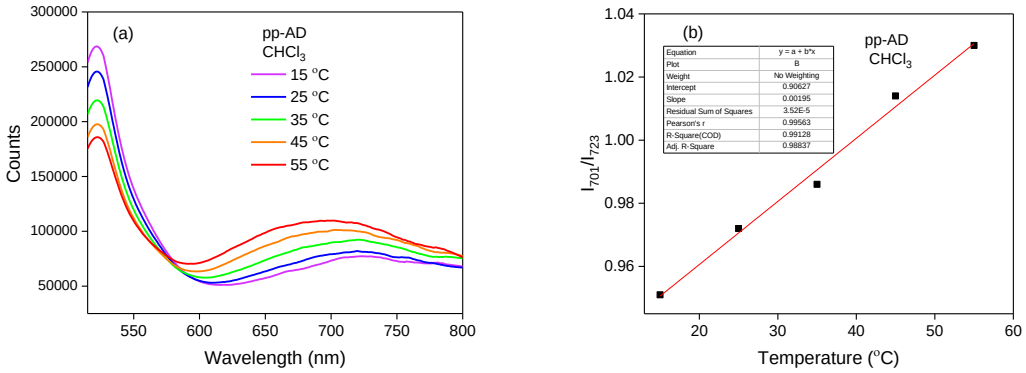

Figure S12. (a) Temperature dependent emission spectra of ***pp*-AD** in $CHCl_3$ and b) Emission intensity ratio with best fit equation at different temperature for ***pp*-AD** in chloroform.

10. Temperature Dependent UV/Vis Absorption Spectra

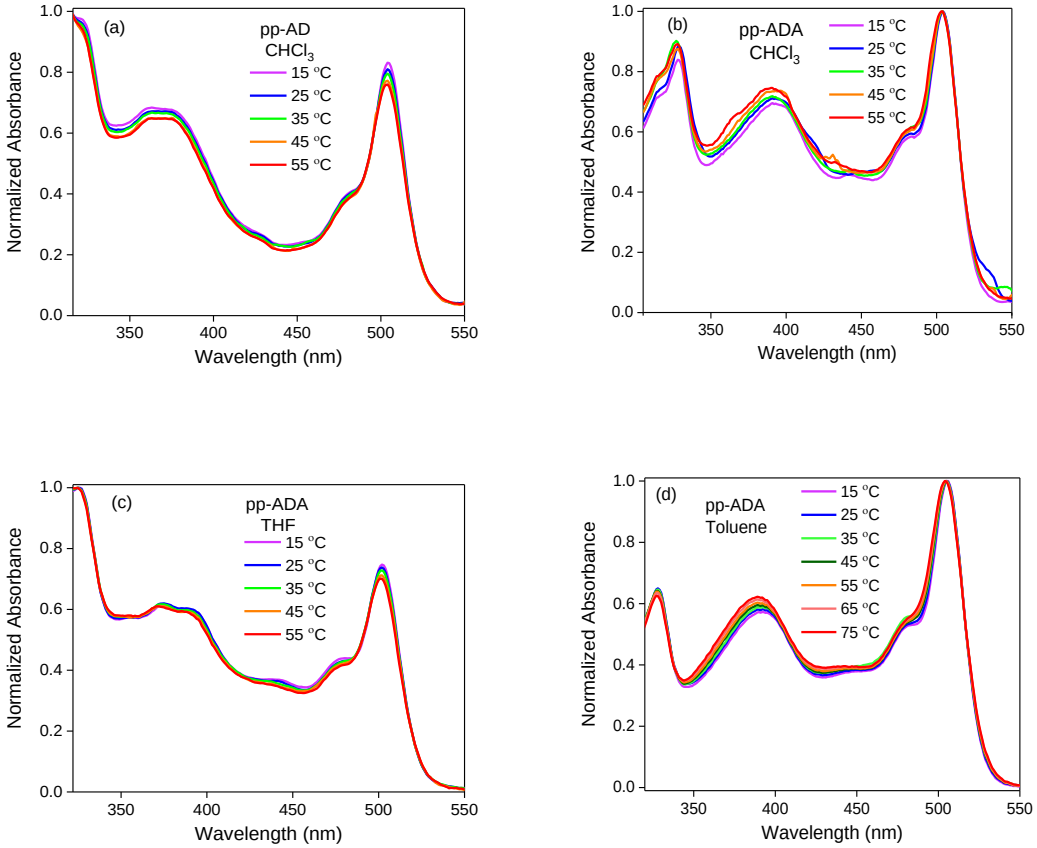

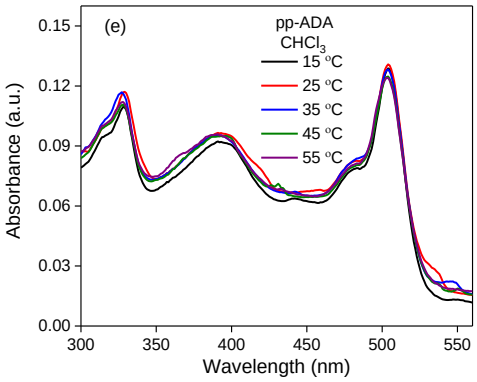

Figure S13. UV/Vis absorption spectra of ***pp*-AD** in (a) $CHCl_3$, and ***pp*-ADA** in (b) $CHCl_3$ (c) THF and (d) Toluene at different temperatures; (e) Unnormalized absorption spectra of ***pp*-ADA** in $CHCl_3$ at variable temperatures.

11. Viscosity sensing

Quantitatively, the viscosity sensitivity of dyad and triads were calculated by using Förster Hoffmann theory[S12, S13]

$$\log (I/I_0) = C + x \log \eta$$

where, I_0 and I are the emission intensities at the initial viscosity i.e., in 100 % MeOH and intensity at different viscosity respectively. The viscosity of the medium is given by η,[S14] C is the experimental temperature and concentration dependent constant and x is the viscosity sensitivity of the molecular rotors.

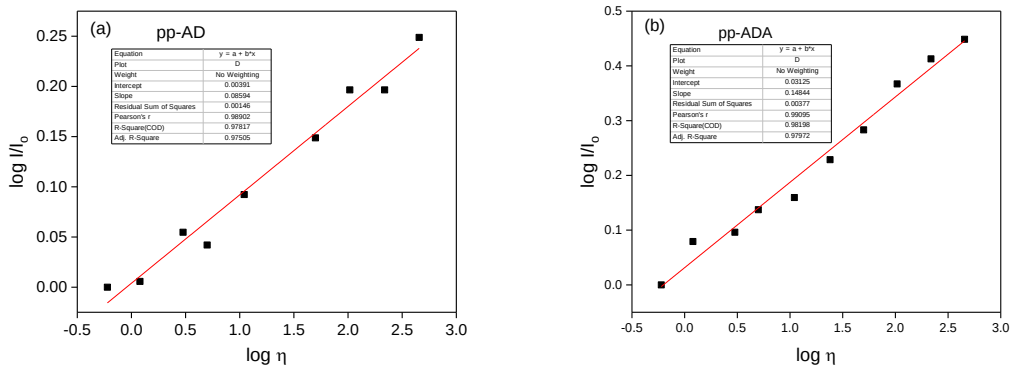

Figure S14. Emission intensity ratio at different viscosities with their best fit equations for (a) ***pp*-AD** and (b) ***pp*-ADA**.

Temperature Dependent Spectra at Particular Viscosity:

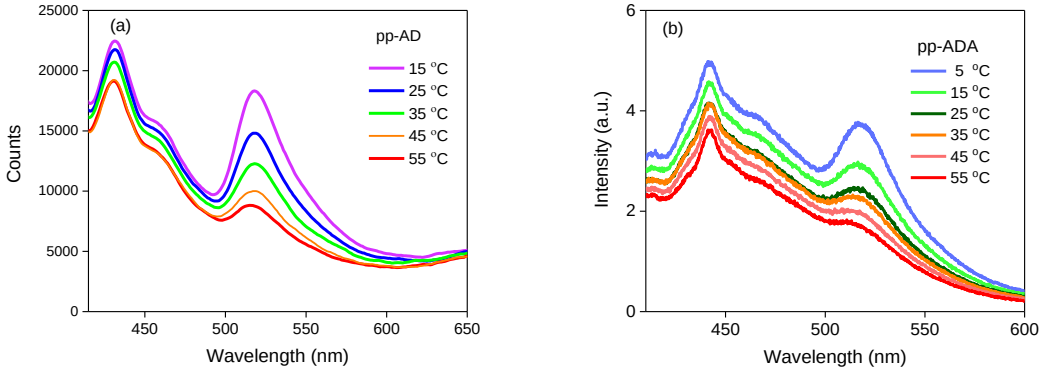

Figure S15. Emission spectra of (a) ***pp*-AD** and (b) ***pp*-ADA** in MeOH:Gly-50:50 (24 cP) at variable temperature.

12. Fluorescence Lifetime

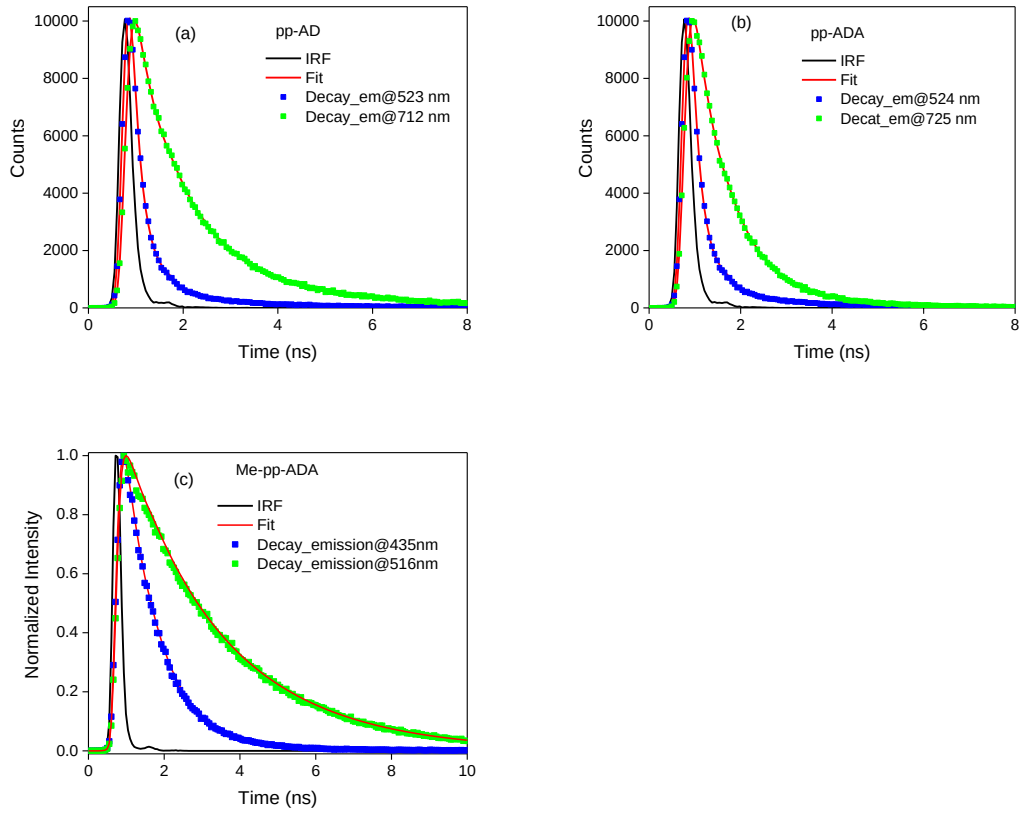

Figure S16. Fluorescence lifetime decay collected by using a single photon counting technique at different wavelengths in $CHCl_3$ samples of (a) ***pp*-AD**, (b) ***pp*-ADA** and (c) **Me-*pp*-ADA**.

Table S6: Fluorescence life time analysis of ***pp*-AD**, ***pp*-ADA** and **Me-*pp*-ADA** at different emission wavelength.

Compound (λ_{ex} = 375nm)	λ_{em} (nm)	$\tau_1(\alpha_1)$ (ns)	$\tau_2(\alpha_2)$ (ns)	$\tau_3(\alpha_3)$ (ns)	τ_{avg} (ns)	χ^2
***pp*-AD**	523	0.38 (0.08)	0.05 (0.92)	2.52 (0.01)	0.09	1.01
	712	0.11 (0.51)	1 (0.41)	2.94 (0.08)	0.69	1.05
***pp*-ADA**	524	0.34 (0.01)	0.03 (0.99)	2.88 (0)	0.03	1.17
	714	0.08 (0.52)	0.75 (0.46)	2.52 (0.02)	0.44	1.06
Me-*pp*-ADA	435	0.86 (0.99)	4.63 (0.01)	-	0.61	0.89
	516	0.93 (0.11)	2.72 (0.89)	-	0.9	1.12

For ***pp*-AD** and ***pp*-ADA**, the decay corresponding to TICT exhibited a longer lifetime than the donor or acceptor emission because TICT requires equilibration of molecules and it is well known that such charge transfer emissions are slower processes compared to normal S_1-S_0 emission.[S2] Furthermore, all the decay profiles could be fitted with tri-exponential functions that indicative of the presence of multiple conformers or species in solution. For **Me-*pp*-ADA,** decay profile corresponding to the emission bands at 435 nm (donor channel) showed a faster decay (τ_{avg} ~ 0.61 ns) than the acceptor decay at 516 nm (τ_{avg} ~ 0.9 ns).

13. Fluorescence Lifetime at Variable Viscosity

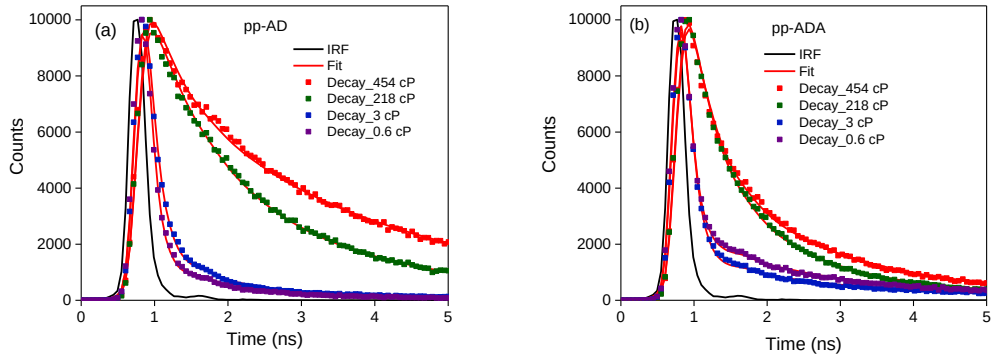

Figure S17. Fluorescence lifetime decay collected at excitation wavelength of 390 nm in $CHCl_3$ samples of (a) ***pp*-AD** and (b) ***pp*-ADA** at 524 nm emission wavelength for both.

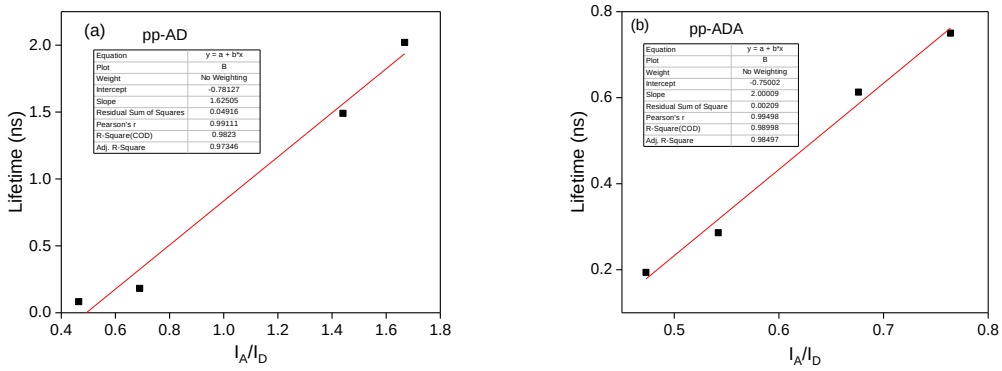

Figure S18. Fluorescence lifetimes at different viscosities and emission intensity ratio of donor and acceptor (I_A/I_D) obtained from steady state emission in (a) ***pp*-AD** and (b) ***pp*-ADA** with their best fit equations.

Table S7: Fluorescence decay parameters of ***pp*-AD** and ***pp*-ADA** at variable viscosity, the decay times (τ_1, τ_2 and τ_3) and the respective fractional contributions (α_1, α_2 and α_3), the amplitude average decay time (τ_{avg}) and the quality of fitting (χ^2).

Compound (λ_{ex} = 375nm)	**Viscosity (in cP) (solvent mixture)**	**$\tau_1(\alpha_1)$ (ns)**	**$\tau_2(\alpha_2)$ (ns)**	**$\tau_3(\alpha_3)$ (ns)**	**Average lifetime τ_{avg} (ns)**	**χ^2**
***pp*-AD**	454 (90/10 v/v gly/MeOH)	0.41 (0.42)	2.87 (0.55)	11.3 (0.02)	2.02	1.35
	218 (80/20 v/v gly/MeOH)	0.65 (0.52)	2.1 (0.46)	10.3 (0.02)	1.49	1.18
	50 (60/40 v/v gly/MeOH)	1.16 (0.17)	8.11 (0.01)	0.25 (0.82)	0.48	1.37
	11 (40/60 v/v gly/MeOH)	0.90 (0.06)	7.41 (0)	0.11 (0.94)	0.18	1.28
	3 (20/80 v/v gly/MeOH)	0.94 (0.03)	7.17 (0)	0.07 (0.97)	0.11	1.50
	0.6 (0/100 v/v gly/MeOH)	0.89 (0.02)	6.33 (0)	0.06 (0.98)	0.08	1.26
***pp*-ADA**	454 (90/10 v/v gly/MeOH)	0.33 (0.69)	1.78 (0.3)	9.02 (0.01)	0.87	1.43
	218 (80/20 v/v gly/MeOH)	1.35 (0.3)	0.34 (0.68)	8.69 (0.01)	0.75	1.14
	50 (60/40 v/v gly/MeOH)	1.31 (0.19)	8.93 (0.01)	0.34 (0.8)	0.61	1.26
	11 (40/60 v/v gly/MeOH)	1.64 (0.05)	0.14 (0.94)	9.51 (0.01)	0.28	1.43
	3 (20/80 v/v gly/MeOH)	1.65 (0.03)	9.16 (0.01)	0.09 (0.96)	0.19	1.33
	0.6 (0/100 v/v gly/MeOH)	1.63 (0.04)	8.19 (0.01)	0.08 (0.95)	0.20	1.17

14. Frequencies and Coordinates of DFT Optimized Geometries

Table S8: Results of first three frequencies and molecular symmetries calculated from geometry optimization of dyad and triads.

Compound	Symmetry	First Three Frequencies
***pp*-AD**	C_1	9.67 10.81 12.92
***pp*-ADA**	C_1	3.91 7.20 7.96
Me-*pp*-ADA	C_1	3.55 5.39 6.46

Coordinates of geometry optimized structure of *pp*-AD

C	-9.20754	-1.34737	-2.09146
C	-8.09981	-1.81675	-2.82498
N	-8.79732	-0.66075	-1.01504
C	-6.96473	-1.37939	-2.15542
C	-7.40349	-0.66158	-1.00986
C	-6.68201	-0.00842	0.00667
C	-7.36984	0.66094	1.03601
C	-6.89515	1.28246	2.22286
N	-8.76176	0.72049	1.05088
C	-8.00747	1.71768	2.93085
C	-9.13775	1.34691	2.17537
C	-0.88100	-0.10331	0.00534
C	-0.16823	-1.13621	0.63693
C	-0.13751	0.90697	-0.63076
C	1.22144	-1.15604	0.64004
C	1.25076	0.88426	-0.63810
C	1.96452	-0.14485	0.00498
B	-9.72570	0.15049	-0.04529
F	-10.66080	-0.68368	0.53629

F	-10.32720	1.18660	-0.73656
H	-8.14364	-2.39763	-3.73497
H	-0.70862	-1.91618	1.16437
H	-0.65573	1.69918	-1.16237
H	1.73841	-1.95227	1.16709
H	1.79268	1.65667	-1.17390
C	3.42986	-0.14731	0.00688
C	4.27203	0.91825	-0.15271
S	4.32795	-1.65955	0.23186
C	5.86019	-0.81278	0.11553
C	5.66151	0.57692	-0.09842
H	3.93079	1.93840	-0.27816
C	6.77549	1.44515	-0.22097
C	8.04633	0.85535	-0.12593
C	8.24428	-0.53502	0.08368
C	7.12971	-1.40211	0.21002
S	9.58159	1.70141	-0.24558
C	10.45268	0.19926	-0.01606
C	9.63993	-0.87628	0.14147
H	9.99339	-1.88835	0.29511
C	6.61407	2.84237	-0.43047
C	7.28978	-2.79948	0.42292
C	6.49214	4.03663	-0.60928
C	7.41376	-3.99298	0.60447
C	6.35265	5.47182	-0.82346
H	7.33332	5.95497	-0.88944
H	5.80194	5.94452	-0.00223
H	5.81237	5.68455	-1.75299
C	7.55819	-5.42713	0.82241
H	8.06924	-5.63570	1.76924
H	8.14027	-5.89408	0.01980
H	6.58025	-5.91917	0.85533

C	-2.36231	-0.08057	0.00539
C	-3.10826	-1.26917	-0.07989
C	-3.07051	1.13076	0.09203
C	-4.46082	1.15481	0.09882
C	-4.49863	-1.24967	-0.08563
C	-5.20128	-0.03604	0.00562
H	-5.05057	-2.18189	-0.14296
H	-2.59171	-2.22004	-0.16490
H	-2.52433	2.06484	0.17808
H	-4.98394	2.10334	0.15998
H	-8.02280	2.22786	3.88316
H	-5.93487	-1.53604	-2.43955
H	-10.26264	-1.46391	-2.29753
H	-10.18596	1.49503	2.39561
H	11.53421	0.21408	-0.01309
H	-5.85831	1.36699	2.51250

Coordinates of geometry optimized structure of *pp*-ADA

C	-16.16008	1.70546	1.81345
C	-15.05251	2.30405	2.44636
N	-15.74954	0.83367	0.88087
C	-13.91724	1.75351	1.86673
C	-14.35571	0.83650	0.87320
C	-13.63430	0.01078	-0.00893
C	-14.32193	-0.83490	-0.89918
C	-13.84763	-1.65775	-1.95671
N	-15.71370	-0.89859	-0.90077
C	-14.96007	-2.21412	-2.57374
C	-16.09009	-1.71631	-1.89462
C	-7.83348	0.11148	-0.03198
C	-7.12254	1.01339	-0.84135
C	-7.08828	-0.76544	0.77659
C	-5.73295	1.03448	-0.84878

C	-5.70005	-0.74010	0.77858
C	-4.98827	0.15635	-0.04106
B	-16.67616	-0.14837	0.08234
F	-17.62428	0.55772	-0.63218
F	-17.26089	-1.04784	0.95537
H	-15.09660	3.04242	3.23394
H	-7.66438	1.68372	-1.50133
H	-7.60514	-1.44847	1.44368
H	-5.21735	1.72240	-1.51209
H	-5.15670	-1.40154	1.44540
C	-3.52313	0.16052	-0.04394
C	-2.67900	-0.85938	0.30063
S	-2.62737	1.61078	-0.53095
C	-1.09413	0.80020	-0.26760
C	-1.29091	-0.53072	0.18715
H	-3.01901	-1.84198	0.60350
C	-0.17480	-1.36255	0.46178
C	1.09358	-0.79675	0.26507
C	1.29039	0.53416	-0.18962
C	0.17430	1.36596	-0.46436
S	2.62678	-1.60725	0.52878
C	3.52266	-0.15706	0.04153
C	2.67850	0.86278	-0.30318
H	3.01824	1.84546	-0.60602
C	4.98795	-0.15280	0.03942
C	5.70017	0.74424	-0.77900
C	7.08845	0.76858	-0.77724
C	7.83318	-0.10719	0.03283
C	7.12177	-1.00858	0.84224
C	5.73217	-1.03132	0.84703
H	5.15693	1.42017	-1.43124
H	7.60512	1.49010	-1.40265

H	5.21636	-1.73370	1.49485
H	7.66378	-1.71693	1.46107
C	14.33271	0.80371	0.93101
C	13.63427	-0.00658	0.01661
C	13.86864	1.70292	1.92916
C	14.98852	2.24292	2.54739
C	16.11241	1.68138	1.90938
C	14.34501	-0.80578	-0.89805
C	13.89597	-1.78682	-1.82348
C	15.02387	-2.33516	-2.41920
C	16.13794	-1.69235	-1.84336
N	15.73744	-0.78456	-0.94138
N	15.72619	0.82844	0.94937
H	15.01211	2.95949	3.35571
B	16.67702	0.13324	-0.08661
F	17.62101	-0.63537	0.56627
F	17.26715	1.09146	-0.89074
C	-0.33377	-2.70114	0.91483
C	0.33347	2.70456	-0.91732
C	-0.45518	-3.84535	1.30096
C	0.45544	3.84875	-1.30334
C	-0.59486	-5.22063	1.76378
H	0.38255	-5.70830	1.84332
H	-1.20777	-5.81136	1.07362
H	-1.07002	-5.26190	2.75055
C	0.59599	5.22401	-1.76594
H	1.06218	5.26461	-2.75702
H	1.21751	5.81161	-1.08084
H	-0.38027	5.71545	-1.83594
C	9.31463	-0.08268	0.02926
C	10.03513	0.17257	-1.15059
C	11.42555	0.19096	-1.15703

C	12.15347	-0.03335	0.02398
C	11.43837	-0.28525	1.20720
C	10.04815	-0.31439	1.20601
H	9.49941	0.33624	-2.08031
H	11.95821	0.39687	-2.07951
H	9.52177	-0.49829	2.13729
H	11.98068	-0.47661	2.12710
C	-9.31481	0.08730	-0.02654
C	-10.06216	1.27068	-0.15875
C	-10.02134	-1.12035	0.10993
C	-11.41165	-1.14677	0.10937
C	-11.45251	1.25095	-0.14797
C	-12.15354	0.04026	-0.01522
H	-12.00564	2.17734	-0.26106
H	-9.54687	2.22173	-0.24917
H	-9.47409	-2.05390	0.19488
H	-11.93360	-2.09113	0.22272
H	-14.97580	-2.88589	-3.41985
H	15.05986	-3.11383	-3.16740
H	-12.81105	-1.79072	-2.22862
H	-17.13832	-1.90324	-2.08287
H	-12.88746	1.96234	2.11538
H	-17.21521	1.85554	1.99638
H	12.86502	-2.05746	-1.99669
H	17.19100	-1.84953	-2.03193
H	17.16288	1.86232	2.09120
H	12.83288	1.91878	2.14483

Coordinates of geometry optimized structure of Me-*pp*-ADA

C	-16.13172	-0.28207	2.53659
C	-14.99883	-0.34489	3.37377
N	-15.72646	-0.15088	1.25927
C	-13.85977	-0.24907	2.58311

C	-14.32712	-0.12483	1.23122
C	-13.64533	0.00460	0.00984
C	-14.34371	0.10950	-1.20448
C	-13.89484	0.25078	-2.56094
N	-15.74332	0.08526	-1.21833
C	-15.04455	0.30569	-3.33999
C	-16.16592	0.20191	-2.49143
C	-7.83441	0.10314	-0.01526
C	-7.12523	1.15284	-0.62219
C	-7.08708	-0.92191	0.59147
C	-5.73543	1.17576	-0.62869
C	-5.69861	-0.89791	0.59403
C	-4.98874	0.14932	-0.02326
B	-16.67080	-0.05036	0.02516
F	-17.48675	1.07413	0.13776
F	-17.44508	-1.20466	-0.07943
H	-15.02464	-0.45021	4.45020
H	-7.66915	1.94568	-1.12639
H	-7.60274	-1.72877	1.10325
H	-5.22146	1.98683	-1.13579
H	-5.15360	-1.68365	1.10696
C	-3.52340	0.15446	-0.02876
C	-2.67812	-0.91385	0.09546
S	-2.62884	1.67490	-0.20587
C	-1.09467	0.82863	-0.11863
C	-1.29022	-0.56768	0.05094
H	-3.01725	-1.93812	0.18861
C	-0.17311	-1.43709	0.14656
C	1.09483	-0.84187	0.07013
C	1.29039	0.55436	-0.09997
C	0.17329	1.42374	-0.19578
S	2.62903	-1.68783	0.16027

C	3.52353	-0.16737	-0.01680
C	2.67836	0.90067	-0.14346
H	3.01753	1.92495	-0.23642
C	4.98906	-0.16150	-0.01747
C	5.70035	0.87990	-0.64260
C	7.08884	0.90571	-0.63363
C	7.83435	-0.11107	-0.01131
C	7.12373	-1.15540	0.60302
C	5.73394	-1.18068	0.60211
H	5.15618	1.66987	-1.14996
H	7.60553	1.73647	-1.10450
H	5.21850	-1.99726	1.09878
H	7.66711	-1.97018	1.07155
C	14.31014	1.14459	0.48536
C	13.64522	0.00180	0.01061
C	13.82410	2.39072	1.00720
C	14.95225	3.14142	1.31629
C	16.09673	2.38291	0.99532
C	14.36035	-1.11280	-0.45779
C	13.93019	-2.37788	-0.98325
C	15.09071	-3.08209	-1.28158
C	16.20044	-2.27749	-0.95071
N	15.76022	-1.10364	-0.45957
N	15.70911	1.19244	0.49983
H	14.96317	4.13980	1.73296
B	16.67044	0.06362	0.02402
F	17.47007	-0.36108	1.08369
F	17.46080	0.52104	-1.02904
C	-0.33068	-2.84062	0.31337
C	0.33098	2.82728	-0.36246
C	-0.45105	-4.04001	0.45490
C	0.45167	4.02664	-0.50388

C	-0.58934	-5.48136	0.62372
H	0.38893	-5.97349	0.60586
H	-1.19765	-5.91828	-0.17632
H	-1.06881	-5.72594	1.57846
C	0.59058	5.46796	-0.67250
H	1.06845	5.71252	-1.62805
H	1.20070	5.90419	0.12654
H	-0.38732	5.96075	-0.65268
C	9.31692	-0.08342	-0.00685
C	10.03849	0.38731	-1.11727
C	11.43112	0.41532	-1.11261
C	12.15089	-0.02842	0.00415
C	11.44023	-0.50044	1.11517
C	10.04761	-0.52645	1.10901
H	9.50371	0.71073	-2.00501
H	11.96781	0.77551	-1.98538
H	9.51874	-0.87058	1.99249
H	11.98373	-0.83959	1.99214
C	-9.31688	0.07855	-0.00969
C	-10.06275	1.26258	0.12061
C	-10.02331	-1.13004	-0.13425
C	-11.41595	-1.15490	-0.12766
C	-11.45546	1.24014	0.12576
C	-12.15094	0.03048	0.00233
H	-12.01099	2.16679	0.23616
H	-9.54619	2.20919	0.24607
H	-9.47597	-2.05864	-0.26387
H	-11.94070	-2.09986	-0.23334
H	-15.08505	0.41043	-4.41602
H	15.14606	-4.07932	-1.69743
C	12.41235	2.85681	1.20705
H	11.84730	2.87688	0.27022

H	12.41400	3.86809	1.62252
H	11.85697	2.21053	1.89354
C	17.53329	2.76013	1.14751
H	17.62448	3.76405	1.56659
H	18.04203	2.72328	0.17939
H	18.04786	2.04679	1.79848
C	17.65247	-2.59610	-1.08928
H	17.78826	-3.59456	-1.50932
H	18.14969	-2.54103	-0.11605
H	18.14421	-1.86103	-1.73367
C	12.54043	-2.90101	-1.19559
H	12.58689	-3.91193	-1.60929
H	11.96591	-2.27871	-1.88847
H	11.96776	-2.94269	-0.26414
C	-12.45526	-0.27741	3.10917
H	-11.90898	0.64232	2.87863
H	-11.87240	-1.10156	2.68694
H	-12.47149	-0.39659	4.19583
C	-17.57360	-0.34393	2.91901
H	-17.68022	-0.44492	4.00078
H	-18.06304	-1.18916	2.42554
H	-18.09548	0.55796	2.58505
C	-17.61286	0.21128	-2.85938
H	-17.73396	0.31195	-3.93964
H	-18.12852	1.03584	-2.35776
H	-18.09742	-0.71070	-2.52393
C	-12.49763	0.33026	-3.10101
H	-12.52903	0.44799	-4.18748
H	-11.91557	-0.56852	-2.87551
H	-11.94135	1.17567	-2.68498

15. References

S1) P. R. Aswathy, S. Sharma, N. P. Tripathi and S. Sengupta, *Chem. Eur. J.*, 2019, **25**,

14870-14880.

S2) D. Simoni, G. Giannini, M. Roberti, R. Rondanin, R. Baruchello, M. Rossi, G. Grisolia, F. P. Invidiata, S. Aiello, S. Marino, S. Cavallini, A. Siniscalchi, N. Gebbia, L. Crosta, S. Grimaudo, V. Abbadessa, A. Di Cristina and M. Tolomeo, *J. Med. Chem.*, 2005, **48**, 4293–4299.

S3) E. Maxima, C. Thivierge, A. Loudet and K. Burgess, *Macromolecules*, 2011, **44**, 4012-4015.

S4) N. Kaur, N. Van Steerteghem, P. Singla, P. Kaur, K. Clays and K. Singh, *Dalton Trans.*, 2017, **46**, 1124-1133.

S5) S. Sengupta and U. K. Pandey, *Org. Biomol. Chem.*, 2018, **16**, 2033–2038.

S6) Z. R. Grabowski, K. Rotkiewicz, W. Rettig, *Chem. Rev.* 2003, **103**, 3899−4031.

S7) G. Chen, H. Sasabe, Y. Sasaki, H. Katagiri, X. F. Wang, T. Sano, Z. Hong, Y. Yang, and J. Kido, *Chem. Mater.,* 2014, **26**,1356-1364.

S8) F. Liu, T. Wu, J. Cao, S. Cui, Z. Yang, X. Qiang, S. Sun, F. Song, J. Fan, J. Wang and X. Peng, *Chem. Eur. J.,* 2013, **19**, 1548–1553.

S9) A. M. Brouwer, *Pure Appl. Chem*., 2011, **83**, 2213-2228.

S10) M. Sirish, B. G. Maiya, J. Photochem. Photobiol. A: *Chem*. 1995, **85**, 127-135.

S11) Y. Chen, J. W. Y. Lam, R. T. K. Kwok, B. Liu and B. Z. Tang, *Mater. Horizons*, 2019, **6**, 428–433.

S12) D. Su, C. L. Teoh, L. Wang, X. Liu, Y. T. Chang, *Chem. Soc. Rev.* 2017**, 46,** 4833 – 4844.

S13) A. Vyšniauskas, M. K. Kuimova, *Int. Rev. Phys. Chem.* 2018**, 37,** 259 –285.

S14) B. Sk, S. Khodia and A. Patra, *Chem. Commun.*, 2018, **54**, 1786-1789.